machines

MDPI

Article

A Novel Dynamic Configuration for Long-Term Fault-Tolerant Operation of Open-End Winding Induction Motors

Mohammed Lamine Belkheiri [1], Abdelkader Beladel [1], Abdellah Kouzou [1,*], Jose Rodriguez [2] and Mohamed Abdelrahem [3,4,*]

[1] Laboratory of Applied Automation and Industrial Diagnostics (LAADI), Faculty of Science and Technology, Ziane Achour University of Djelfa, P.O. Box 3117, Djelfa 17000, Algeria; ml.belkheiri@univ-djelfa.dz (M.L.B.); a.beladel@univ-djelfa.dz (A.B.)
[2] Center for Energy Transition, Universidad San Sebastián, Santiago 8420524, Chile; jose.rodriguezp@uss.cl
[3] Department of Electrical Engineering, Faculty of Engineering, Assiut University, Assiut 71516, Egypt
[4] Chair of High-Power Converter Systems, Technical University of Munich, 80333 Munich, Germany
* Correspondence: a.kouzou@univ-djelfa.dz (A.K.); mohamed.abdelrahem@tum.de (M.A.)

Abstract

This paper presents a novel dynamic configuration for ensuring long-term fault-tolerant operation of three-phase open-end winding induction motors (3P-OEWIM). Conventional strategies are limited by their inability to sustain performance under multiple simultaneous failures, particularly when faults affect both inverters or power sources. To address these limitations, this study proposes an integrated topology that combines fault-tolerant techniques from conventional star-connected drives, common DC supply OEWIM, and separate DC supplies OEWIM configurations. The proposed system dynamically reconfigures its power topology in response to fault conditions, maintaining rated power operation whenever possible and transitioning to reduced-power or two-phase modes under compound faults. Simulation results demonstrate that the proposed strategy enhances system resilience against consecutive failures, including combined DC supply and inverter faults. Integrating these multiple strategies into a single dynamic topology improves operational continuity, making 3P-OEWIM drives more resilient for critical applications such as electric vehicles and industrial automation.

Keywords: open-end winding induction motor (OEWIM); fault-tolerant control (FTC); dynamic reconfiguration; consecutive faults; DC supply faults; inverter switch failure; zero-sequence current (ZSC); electric vehicles

Check for updates

Academic Editors: Ahmed Abu-Siada and Maciej Sułowicz

Received: 2 August 2026
Revised: 29 September 2026
Accepted: 3 October 2026
Published: 9 October 2026

Copyright: © 2026 by the authors. Licensee MDPI, Basel, Switzerland. This article is an open access article distributed under the terms and conditions of the Creative Commons Attribution (CC BY) license.

1. Introduction

Three-phase electric machines, particularly those based on induction motors (IMs) and permanent magnet synchronous motors (PMSMs), are widely used in industrial, automotive, and renewable energy applications due to their reliability, efficiency, and cost-effectiveness. However, these machines are susceptible to various faults, such as open-phase faults, inverter switch failures, and DC supply faults, which can lead to significant performance degradation, including torque and speed ripples, increased losses, and even complete system shutdown. To address these challenges, fault-tolerant control (FTC) strategies have been developed to ensure continuous and reliable operation under fault conditions [1–5].

One of the earliest and most influential contributions to fault-tolerant (FT) motor drives was made by [6], who proposed connecting the neutral point of an IM to the midpoint of the

DC link voltage. This approach introduced a Zero-Sequence Current (ZSC) path, allowing the motor to continue operating even after the loss of one inverter leg or motor phase. It was demonstrated that by increasing the currents in the remaining phases to $\sqrt{3}$ times their original magnitude and phase-shifting them by $\pm 30^{\circ}$, the system could maintain the rotating magnetomotive force (RMMF) and eliminate torque pulsations. This strategy laid the foundation for modern FTC in IMs [6–9]. Extending this approach, refs. [10,11] introduced a four-leg inverter topology, where the motor neutral point is connected to an additional inverter leg. This configuration enabled the system to compensate for the lost phase and maintain balanced operation with only two stator windings [12].

Similarly, ref. [13] extended the concept of Stator Neutral Point Connection (SNPC) and proposed an alternative FT strategy known as Stator Phase Connection (SPC) which enhances system performance by connecting the phase corresponding to the faulty inverter leg directly to the DC midpoint, ensuring the preservation of three-phase operation.

Building on these foundational topologies, several studies have further refined FTC strategies for conventional motor drives. Ref. [14] introduced a dynamic strategy that adapts between three-phase and two-phase operation using a four-leg inverter, reducing additional losses by 50% compared to continuous two-phase operation. Ref. [15] compared the three legs-neutral connected to capacitor midpoint (3L-NCM) and three plus one legs-neutral connected to an additional leg ((3 + 1)L-NAL) configuration, demonstrating that the (3 + 1)L-NAL topology maintains higher voltage and current capabilities under fault conditions. Ref. [16] proposed a transformation-matrix-based FTC for PMSMs that maintains 66.7% of rated power during open-phase faults. Ref. [17] improved controlled neutral point strategies to minimize torque ripple in PMSM drives under open-phase faults, while ref. [18] proposed a vector control method based on an Asymmetrical Current Transformation (CT) that enables the use of conventional control techniques for open-phase IMs.

In practice, implementing FTC requires fast and accurate fault detection and isolation (FDI) to identify damaged components before initiating remedial actions. For three-phase voltage-source inverters, various diagnostic methods have been proposed, including stator current signature analysis, such as half-wave current evaluation [19–21], Park's vector monitoring for open-switch localization [22], and hardware-level desaturation circuits for fast isolation of short-circuit faults [23]. In addition, model-based observers and machine learning methods, such as lightweight convolutional neural networks (CNNs), have been applied to classify faults under variable load and noisy conditions [24–27].

While the aforementioned strategies have significantly improved FTC in conventional motor drives, they remain confined to single-inverter topologies. Indeed, the emergence of Open-End Winding (OEW) configurations has introduced a new paradigm in motor drive design. In OEW configurations, rather than forming a traditional wye or delta topology, the stator winding terminals are left unconnected and each end is fed by an independent inverter, offering several advantages over conventional designs.

Compared to traditional Star/Delta and conventional Multilevel Inverter (MLI) topologies, OEW drives naturally generate multilevel voltage waveforms, achieving low Total Harmonic Distortion (THD) and superior voltage availability without the structural complexities of traditional MLIs. Unlike Neutral-Point Clamped (NPC) and Flying Capacitor (FC) converters, OEW drives eliminate neutral-point voltage drift, clamping diodes, and active capacitor-balancing algorithms, and when operating from a single supply, they avoid the strict requirement for multiple isolated DC sources typical of Cascaded H-Bridge (CHB) architectures. These inherent advantages, combined with extensive switching state flexibility, render OEW induction motor (OEWIM) drives exceptionally

resilient for high-reliability applications, including electric vehicles and critical industrial processes [28–41].

OEW motor drive systems are broadly categorized into two configurations: common DC supply and separate DC supplies. Each configuration offers different trade-offs in switching flexibility and fault-tolerance capability.

In the common DC supply topology, circulating ZSC presents a major challenge during normal operation, necessitating active suppression control that reduces the degrees of freedom for redundant switching vectors. However, this natural ZSC path becomes advantageous during open-switch or open-phase faults, providing an inherent zero-sequence conduction route without requiring auxiliary hardware or structural modification [42–50].

Conversely, the separate DC supplies topology avoids circulating ZSCs altogether, eliminating the need for active suppression control. Although this configuration increases system complexity and cost, independent DC links allow the integration of hybrid energy storage units and enable asymmetric voltage ratios to synthesize higher voltage levels with lower harmonic distortion [51–56]. For fault tolerance, this configuration compensates for both single-inverter failures and DC-source outages by short-circuiting the faulty inverter to form an artificial neutral point. Nevertheless, this structure suffers from a critical limitation during complete open-phase faults; due to the absence of a ZSC path, it cannot sustain operation under two-phase conditions, thereby constraining its overall FT capability.

Similar to conventional single-inverter drives, fault diagnosis in dual-inverter OEW configurations relies on signal-based, Park's vector, and observer methods, while addressing the structural symmetry between the two converters [57]. Because symmetric switch pairs on opposing inverters produce similar phase current distortions and zero-sequence signatures, identifying the exact faulty inverter introduces ambiguity. To resolve this, active diagnostic techniques have been developed, including high-frequency voltage pulse injection [58], gate signal reconstruction, and unipolar duty-ratio modulation [57,59,60]. These methods distinguish between the two converters and reliably locate the faulty switch across the operating range.

To sustain post-fault operation, various FTC strategies have been developed for specific OEW topologies. For common DC bus OEW drives, research has focused on utilizing the inherent ZSC path during faults. Early works developed unified modulation and third-harmonic injection to simplify control under fault conditions [61,62]. For complete phase losses, ref. [63] implemented resonant controllers to track the fundamental ZSC while suppressing harmonic circulating currents, and ref. [64] developed single-sensor current reconstruction to maintain post-fault control in propulsion drives. Under single switch failures, conventional strategies typically deactivate the entire faulty phase leg and operate the machine in two-phase mode using the ZSC return path. To avoid this degradation to two-phase mode, ref. [50] introduced a unipolar modulation strategy that keeps the healthy switch in the faulty leg operating, while ref. [65] developed an adaptive zero-sequence current controller to eliminate post-fault torque ripple. On the other hand, in OEW systems with separate DC sources, fault tolerance relies primarily on neutral-point formation [66]. This principle is widely adopted in electric vehicle (EV) traction drives with dual isolated supplies, where refs. [67] and [60] developed post-fault neutral-point formation strategies using contactor-based isolation and active short-circuit (ASC) gating, respectively, to sustain propulsion under single-inverter failures. More recently, ref. [68] proposed an artificial neural network (ANN)-assisted Duty-DTC strategy with external contactors to minimize post-fault torque ripple, while ref. [69] formulated a software-based virtual neutral point using a fault-indexed ANN to achieve fault tolerance without auxiliary isolation contactors. Alternatively, refs. [70,71] explored active space-vector modulation to

maintain continuous dual-inverter operation without hardware isolation specifically under single-switch short-circuit conditions.

Despite these advancements in OEW fault tolerance, both configurations still face significant limitations. In common DC supply drives, several operational challenges remain. First, during healthy operation, active suppression of circulating ZSC is required, which reduces switching flexibility. Second, under a single switch failure, conventional strategies conservatively treat the fault as a complete phase outage, unnecessarily forcing the drive into two-phase operation, which severely restricts torque capability to 57.7% and increases conduction losses. Third, although recent unipolar modulation strategies avoid this over-isolation, they still experience derated power capability and require continuous zero-sequence regulation. Most critically, because both inverters share a single DC link, this topology provides no supply redundancy and cannot compensate for DC supply failures.

In separate DC supplies OEW drives, different limitations arise. First, the absence of a natural ZSC path prevents operation under complete open-phase faults. Second, neutral-point formation isolates the DC supply connected to the faulty inverter, reducing the available voltage and output power by half. Furthermore, this approach fails when faults affect both upper and lower switches, as neither switch group can be entirely closed to form the neutral point. Third, active modulation methods that avoid inverter isolation are restricted only to single-switch short circuits and suffer from reduced voltage utilization, which limits the achievable operating speed.

Additionally, most existing FTC methods address only single inverter faults. They cannot handle consecutive failures across both inverters, nor can they operate when a DC supply fails on one side while an inverter fails on the opposite side.

To overcome these limitations, this work proposes a new dynamic topology for an advanced long-term FTC of 3P-OEWIM that integrates the strengths of three existing FT strategies:

- FTC for conventional star IM.
- FTC for common DC supply OEWIM.
- FTC for separate DC supplies OEWIM.

By integrating multiple established FT topologies, the proposed strategy aims to:

1. Maintain Rated Power: Ensure the motor operates at its rated power level as much as possible, even under multiple switch failures occurring at the same level (upper or lower) or across different levels.
2. Enhance Fault Tolerance: Provide resilience against a wide range of faults, including:
    - Switch failures (open-circuit and short-circuit).
    - Open-phase faults.
    - DC supply failures.
3. Handle Sequential Faults: Manage complex consecutive failure scenarios, such as:
    - Multiple inverter switch failures, encompassing faults from both inverters, rather than just a single inverter.
    - Combined DC supply and inverter failures.
4. Isolate Critical Faults: Effectively isolate severe faults, such as two switches in the same inverter leg being short-circuited, preventing catastrophic failure.

Accordingly, this study hypothesizes that integrating multiple FTC strategies, specifically for conventional star 3P-IM, 3P-OEWIM with a common DC supply, and 3P-OEWIM with separate DC supplies, will result in a significantly improved FT capability compared to existing standalone methods. Simulation results and performance analysis under diverse fault scenarios demonstrate this improvement.

The remainder of this paper is organized as follows: Section 2 presents the modeling of 3P-OEWIM. Section 3 discusses FTC strategies for the 3P-OEWIM, beginning with the conventional 3P-IM and then addressing the OEWIM configuration under both separate and common DC supply configurations. This section also introduces the proposed dynamic topology. Section 4 presents the simulation results, quantitative benchmark comparisons, and discussion to validate the effectiveness of the proposed approach. Finally, Section 5 concludes the paper.

2. Three-Phase OEWIM Modelling

The three-phase open-end winding induction motor (3P-OEWIM) drive is established by opening the stator neutral connection and feeding the stator windings from both ends using two two-level voltage source inverters. This arrangement is implemented in two primary DC-link configurations, as illustrated in Figure 1:

- Dual-inverter OEWIM with separate isolated DC supplies (Figure 1a), which employs an independent DC source for each inverter, providing galvanic isolation and eliminating zero-sequence circulating currents.
- Dual-inverter OEWIM with a common DC supply (Figure 1b), which utilizes a single shared DC source across both inverters, reducing source hardware while creating a path for zero-sequence currents.

The mathematical model of the healthy 3P-OEWIM is developed in both the *abc* and $\alpha\beta$ reference frames.

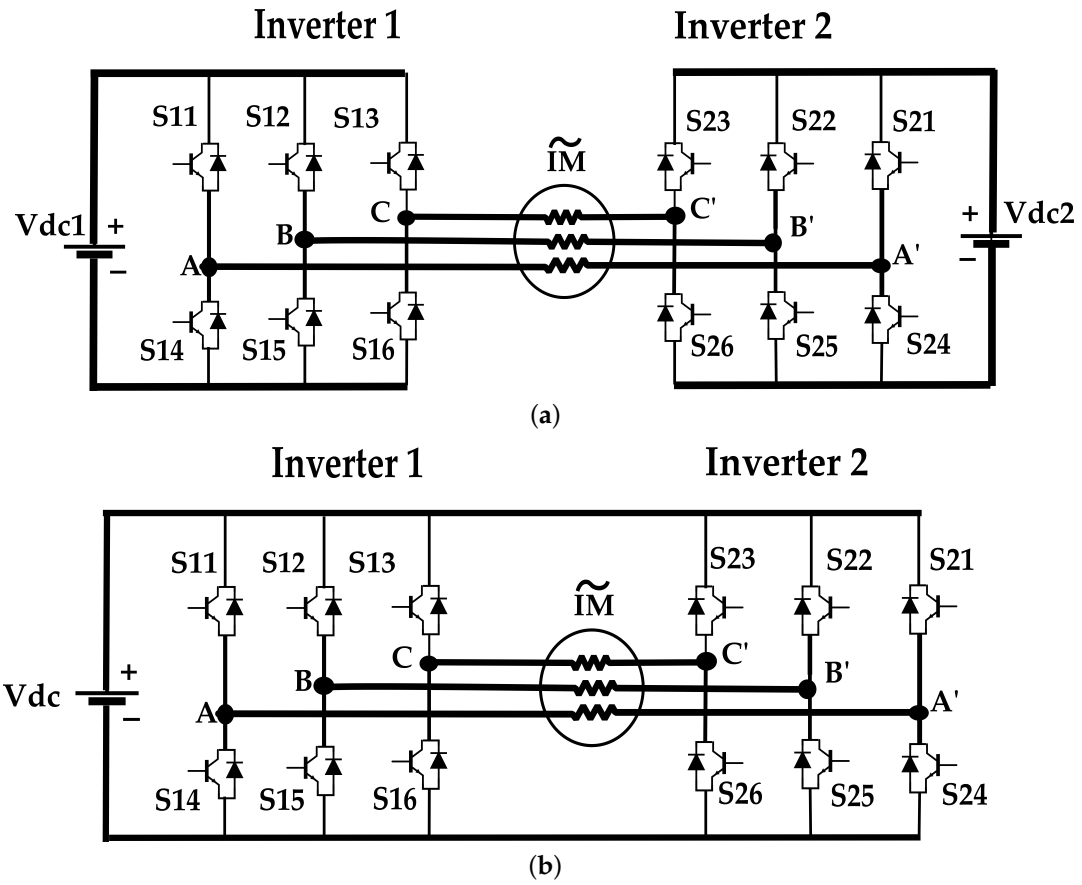


Figure 1. Dual two-level inverter-fed open-end winding induction motor (OEWIM) configurations: (**a**) with separate isolated DC supplies; (**b**) with a common DC supply.

2.1. Voltage Equations in the abc Frame

The stator voltage vector in the *abc* reference frame is expressed as:

$$v_{abc,s} = \begin{bmatrix} v_{as} \\ v_{bs} \\ v_{cs} \end{bmatrix} \tag{1}$$

For the OEW configuration, the effective stator voltage is the difference between the voltages of the two inverters:

$$v_{abc,s} = v_{inv1} - v_{inv2} \tag{2}$$

where

$$v_{inv1} = \begin{bmatrix} v_{a1} \\ v_{b1} \\ v_{c1} \end{bmatrix}, \quad v_{inv2} = \begin{bmatrix} v_{a2} \\ v_{b2} \\ v_{c2} \end{bmatrix} \tag{3}$$

The voltage equations of the stator and rotor are given by:

$$v_{abc,s} = R_s i_{abc,s} + \frac{d\lambda_{abc,s}}{dt} \tag{4}$$

$$v_{abc,r} = R_r i_{abc,r} + \frac{d\lambda_{abc,r}}{dt} \tag{5}$$

where $i_{abc,s} = [i_{as}, i_{bs}, i_{cs}]^T$ is the stator current vector, $i_{abc,r} = [i_{ar}, i_{br}, i_{cr}]^T$ is the rotor current vector, R_s and R_r are the stator and rotor resistances, respectively, and $\lambda_{abc,s}$ and $\lambda_{abc,r}$ denote the stator and rotor flux linkage vectors.

2.2. Flux Linkage Relations

The general flux linkage relationships can be written as:

$$\begin{bmatrix} \lambda_{abc,s} \\ \lambda_{abc,r} \end{bmatrix} = \begin{bmatrix} L_{ss} & L_{sr} \\ L_{rs} & L_{rr} \end{bmatrix} \begin{bmatrix} i_{abc,s} \\ i_{abc,r} \end{bmatrix} \tag{6}$$

where the 3×3 stator and rotor inductance matrices are defined as:

$$L_{ss} = L_s I_3 + M_s J_3, \quad L_{rr} = L_r I_3 + M_r J_3, \quad L_{sr} = L_{rs}^T = L_m I_3 \tag{7}$$

where L_{ss} and L_{rr} denote the 3×3 stator and rotor inductance matrices, respectively. Here, I_3 is the 3×3 identity matrix, J_3 is a 3×3 matrix of ones, L_s and L_r denote the phase self-inductances of the stator and rotor, M_s and M_r represent the inter-phase mutual inductances, and L_m is the magnetizing inductance.

2.3. Clarke Transformation ($abc \rightarrow \alpha\beta$)

To simplify the analysis, the three-phase quantities are transformed into the stationary $\alpha\beta$ reference frame using the Clarke transformation matrix:

$$K = \frac{2}{3} \begin{bmatrix} 1 & -\frac{1}{2} & -\frac{1}{2} \\ 0 & \frac{\sqrt{3}}{2} & -\frac{\sqrt{3}}{2} \end{bmatrix} \tag{8}$$

Any three-phase vector $x_{abc} = [x_a, x_b, x_c]^T$ is transformed as:

$$x_{\alpha\beta} = K x_{abc} \tag{9}$$

Thus, the stator voltages, currents, and flux linkages in the $\alpha\beta$ frame are given by:

$$v_{\alpha\beta} = K v_{abc,s}, \quad i_{\alpha\beta} = K i_{abc,s}, \quad \lambda_{\alpha\beta} = K \lambda_{abc,s} \tag{10}$$

For the OEW motor, the equivalent voltage becomes:

$$v_{\alpha\beta} = v_{\alpha\beta,1} - v_{\alpha\beta,2} \tag{11}$$

2.4. Voltage Equations in the αβ Frame

In the stationary two-axis $\alpha\beta$ frame, the voltage equations are expressed as:

$$\begin{bmatrix} v_\alpha \\ v_\beta \end{bmatrix} = R_s \begin{bmatrix} i_\alpha \\ i_\beta \end{bmatrix} + \frac{d}{dt} \begin{bmatrix} \lambda_\alpha \\ \lambda_\beta \end{bmatrix} \tag{12}$$

or, equivalently, in vector form:

$$v_{\alpha\beta} = R_s i_{\alpha\beta} + \frac{d\lambda_{\alpha\beta}}{dt} \tag{13}$$

2.5. Electromagnetic Torque

The electromagnetic torque is expressed in the $\alpha\beta$ reference frame as:

$$T_e = \frac{3}{2} P (\lambda_\alpha i_\beta - \lambda_\beta i_\alpha) \tag{14}$$

where P is the number of pole pairs.

2.6. Mechanical Dynamics

$$J \frac{d\omega_r}{dt} + F\omega_r = T_e - T_L \tag{15}$$

where J—rotor inertia, F—viscous friction coefficient, ω_r—rotor angular speed, T_L—load torque.

2.7. Inverter Switching States

In dual-inverter OEWIM configurations with either separate DC supplies or a common DC supply, as shown in Figure 1, the switching states of the twelve switches theoretically permit 64 possible configurations. However, because of inherent system redundancies, many of these states produce identical voltage space vectors. As a result, the system effectively generates only 18 distinct active voltage vectors, along with a single null vector, as illustrated in Figure 2.

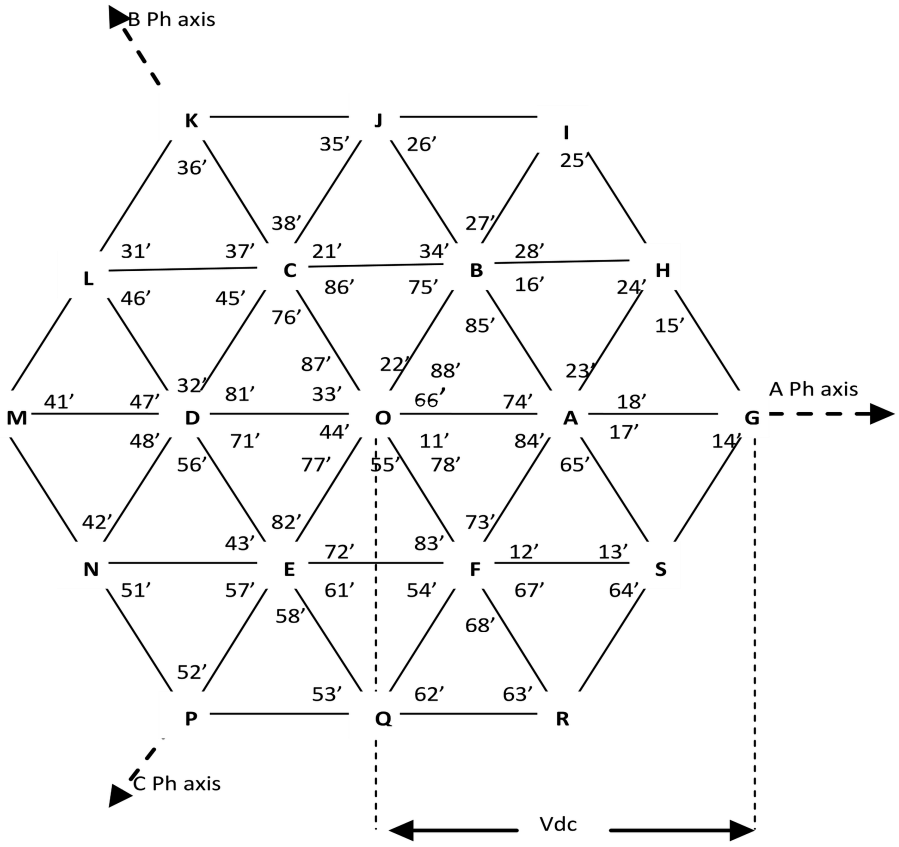


Figure 2. SVPWM diagram of the dual two-level inverter-fed OEWIM.

3. Fault-Tolerant Control of 3P-OEWIM

FTC in three-phase IM (3P-IM) systems is strongly dependent on the converter topology and the available redundancy within the power stage. The nature of fault response differs between conventional 3P-IM structures and OEWIM configurations, particularly in terms of inverter interaction and DC-link utilization.

Different OEWIM configurations exhibit distinct fault management capabilities. In particular, systems with separate DC supplies and those with a common DC supply provide different degrees of flexibility for neutral point formation and post-fault reconfiguration.

3.1. FTC for the Conventional Three-Phase IM

FTC in conventional star-connected 3P-IM systems is commonly implemented by connecting the motor neutral point to a controlled bridge (four-leg inverter). This approach is particularly effective in mitigating the effects of open-phase faults, a common failure mode in inverter-fed drives. An open-phase fault, where one of the three motor phases becomes open-circuited, disrupts the balanced three-phase current flow. Similarly, an open-circuited switch in the inverter can also be considered an open-phase fault and use this technique to mitigate its effects, ensuring continued operation with minimal performance loss.

Without a neutral connection, the current is forced to flow only through the two remaining healthy phases, resulting in identical currents in these windings. This effectively transforms the three-phase motor into a single-phase system with two windings in series, eliminating the necessary phase difference for a RMMF. This leads to a pulsating magnetic field instead, causing significant torque pulsations, mechanical vibrations, noise, and a reduction in average torque. The current imbalance also increases losses in the remaining two phases, leading to overheating.

Connecting the motor neutral point to a fourth leg provides a robust solution to these problems. This configuration allows for controlled injection of current into the neutral point, enabling dynamic current redistribution and mitigating the effects of the open-phase fault.

The fundamental concept of this post-fault control is based on managing the machine stator flux, denoted as $\lambda_{abc,s}$. The total flux within each stator phase consists of two primary components:

- Flux generated by the stator currents: $\lambda_{abc,s}(i_s)$.
- Flux induced by the rotor currents: $\lambda_{abc,s}(i_r)$.

$$\lambda_{abc,s} = \lambda_{abc,s}(i_s) + \lambda_{abc,s}(i_r) \tag{16}$$

Since the rotor currents in a squirrel-cage IM cannot be directly accessed, maintaining the rotor flux linkage requires precise control of the stator currents. Consequently, an effective fault-tolerant strategy ensures that the post-fault stator flux linkage matches healthy operating conditions, thereby stabilizing motor performance.

Using the superposition principle, the portion of the flux that is generated by the stator currents can be expressed using the stator inductance matrix L_{ss} as:

$$\lambda_{abc,s}(i_s) = L_{ss} i_{abc,s} = (L_s I_3 + M_s J_3) i_{abc,s} \tag{17}$$

where the stator phase self-inductance L_s and inter-phase mutual inductance M_s are defined in terms of the stator leakage inductance L_{ls} and magnetizing inductance L_m as:

$$L_s = L_{ls} + \frac{3}{2} L_m, \quad M_s = -\frac{1}{2} L_m \tag{18}$$

Applying the Clarke transformation, the stator flux components in the $\alpha\beta$-reference frame can be rewritten in terms of the stator currents as:

$$\lambda_{\alpha s}(i_s) = L_s \frac{2i_{as} - i_{bs} - i_{cs}}{3}, \quad \lambda_{\beta s}(i_s) = L_s \frac{i_{bs} - i_{cs}}{\sqrt{3}} \tag{19}$$

Assuming that phase a is the faulted phase, it becomes open-circuited, making its current zero ($i_{as} = 0$). Under this condition, the flux linkage equations take the form:

$$\hat{\lambda}_{\alpha s}(i_s) = -L_s \frac{\hat{i}_{bs} + \hat{i}_{cs}}{3}, \quad \hat{\lambda}_{\beta s}(i_s) = L_s \frac{\hat{i}_{bs} - \hat{i}_{cs}}{\sqrt{3}} \tag{20}$$

where $\hat{}$ represents post-fault values.

To maintain the same flux as in the healthy condition, the above equation must match the pre-fault case. This leads to the following expressions for the post-fault phase currents:

$$\hat{i}_{bs} = 2i_{bs} + i_{cs} = i_{bs} - i_{as}, \quad \hat{i}_{cs} = i_{bs} + 2i_{cs} = i_{cs} - i_{as} \tag{21}$$

These equations demonstrate that after a fault, the remaining two-phases currents become $\sqrt{3}$ times larger than in normal operation and shift their phase by 60°, allowing the machine to function in two-phase mode while preserving torque generation.

By substituting the modified post-fault currents into the flux equations, the new stator flux expression for the faulted motor is:

$$\hat{\lambda}_{abc,s} = \lambda_{abc,s} - L_{ls} i_{as} \tag{22}$$

Substituting these equations into the general voltage equation results in the post-fault stator voltage equations:

$$\hat{v}_{abc,s} = v_{abc,s} - \left(R_s + L_{ls}\frac{d}{dt}\right) i_{as}, \quad \hat{v}_{abc,r} = v_{abc,r} \tag{23}$$

The stator voltages in the faulted condition remain equal to those in the healthy case, with an additional compensation term to account for the missing phase current.

Additionally, the voltage at the neutral point can be expressed as:

$$v_{za} = v_{as} - E_{as} = R_s i_{as} + L_{ls}\frac{d}{dt} i_{as} \tag{24}$$

where v_{za} is the voltage at the neutral point and E_{as} denotes the back electromotive force (back-EMF) induced in phase a.

The post-fault control strategy relies on modifying the magnitude and phase shift of the two remaining phase currents to maintain a constant machine flux. This two-phase operation mode requires a ZSC path to balance the system, where current redistribution is directly linked to adjusting the neutral point voltage and regulating the active phase voltages. Consequently, torque continuity is preserved with minimal performance degradation [14,15].

The system consists of a three-phase inverter and an auxiliary bridge, which includes a pair of switches connected to the neutral point and the positive and negative poles of the DC supply, as shown in Figure 3.

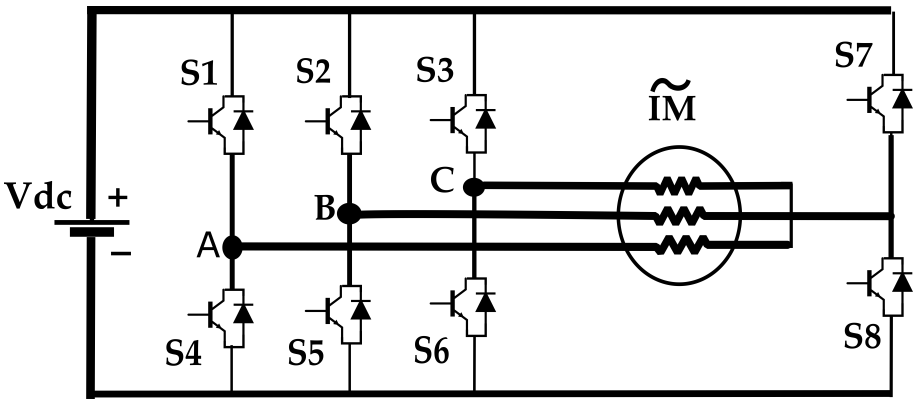


Figure 3. The (3 + 1)L-NAL fault-tolerant topology with controlled neutral point.

Consequently, the system is reconfigured such that the two active phases of the motor are controlled by three inverter legs. In a two-phase framework, a single open switch is treated as an open-phase fault. Alternatively, this configuration can be operated within a three-phase framework, where a single open switch is not classified as a full phase loss; instead, the system is divided into faulty and healthy conduction paths based on the current direction in the affected inverter arm [14].

3.2. FTC for the OEWIM

In OEWIM systems, fault-tolerant operation depends on the DC-link arrangement, which determines the available post-fault reconfiguration strategy.

3.2.1. FTC in OEWIM with Separate DC Supplies

In the OEWIM configuration fed by two separate DC sources, each inverter independently supplies one side of the stator windings. If an open-circuit or short-circuit fault occurs in any inverter switch, the system reconfigures using the remaining healthy switches to form a neutral point, effectively transforming the machine into a conventional star-connected motor. This is achieved by closing either all three upper or all three lower

switches to generate the zero voltage vectors (111) or (000). Consequently, the voltage supplied to the windings is derived from only one active inverter.

Under this fault scenario, the available output power is reduced to half of the rated capacity. As illustrated by the red lines in Figure 4, the Space Vector Pulse Width Modulation (SVPWM) control transitions to that of a conventional two-level inverter operating with a single DC supply. This reconfiguration strategy can also be deployed if one of the DC supplies fails; by shutting down the corresponding inverter and utilizing it as a neutral point, the system ensures operational continuity and fault-tolerant capability, albeit at a reduced power level.

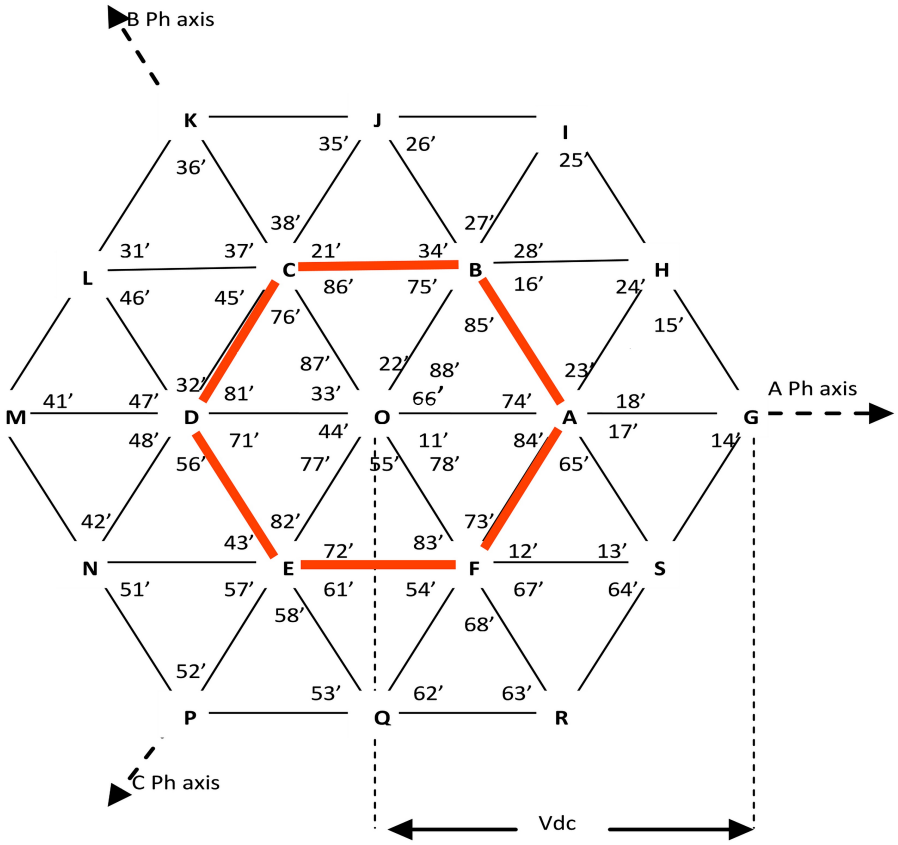


Figure 4. SVPWM diagram under FTC for OEWIM with separate DC supplies.

3.2.2. FTC in OEWIM with Common DC Supply

In this configuration, both inverters are connected to a single DC source through a common DC link, where fault-tolerant operation is facilitated by a ZSC path without requiring auxiliary hardware. If the system experiences an open-circuit fault in either a switch or an entire phase, it remains capable of generating an RMMF utilizing the remaining two healthy phases.

Under this scenario, the SVPWM transitions to a two-phase system. If phase *c* becomes open-circuited, all voltage vectors containing a switching state of '1' for phase *c* are effectively reduced to '0'. Figure 5 illustrates the newly available voltage vectors (highlighted by the red lines) under a phase *c* open-circuit fault. Consequently, this asymmetrical configuration necessitates a modified rotational coordinate system to successfully obtain decoupled voltages in the *d*-*q* axis equations.

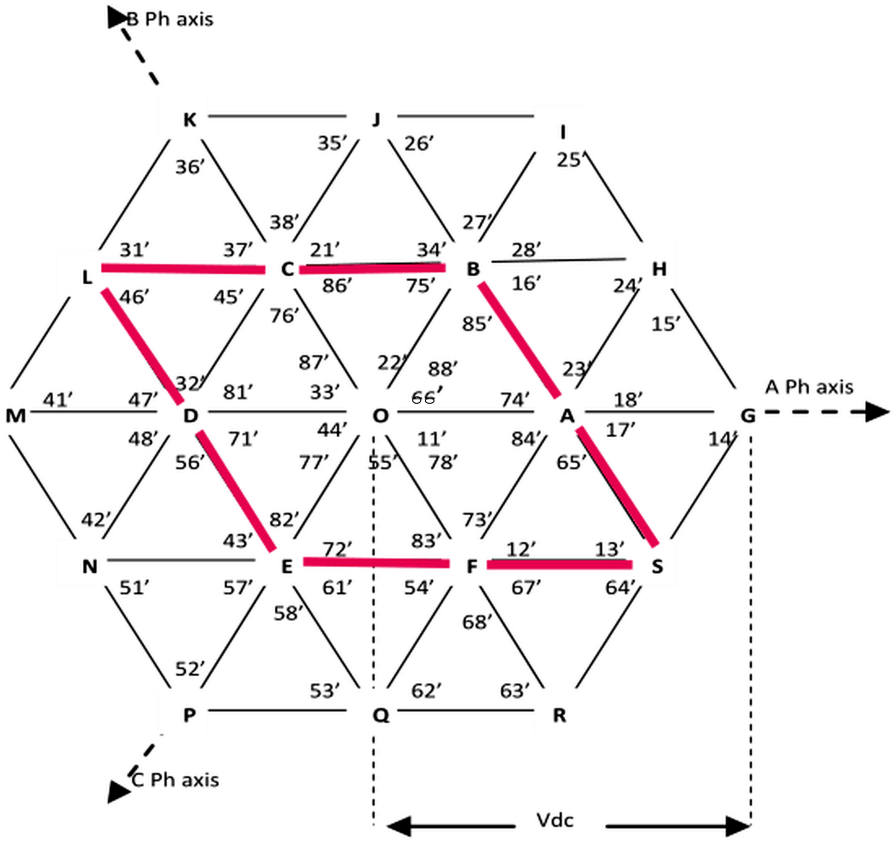


Figure 5. SVPWM diagram under FTC for OEWIM with a common DC supply.

3.3. The Proposed Dynamic Topology

The proposed dynamic topology integrates three FT configurations into a unified reconfigurable architecture: the neutral-point-controlled star connection, single-inverter operation with separate DC supplies, and two-phase ZSC-based operation under a common DC bus. As faults accumulate, the system sequentially activates the appropriate reconfiguration mechanism, transitioning between these configurations to maintain continuous operation.

Figure 6 illustrates the proposed dynamic topology for the OEWIM system. The key components of this architecture are:

- Dual Inverters: Two independent inverters are connected to both ends of the motor stator windings. In this arrangement, each inverter is powered by a separate DC supply, conforming to the conventional OEWIM configuration to ensure a balanced power distribution across the machine.
- SPDT Switches: The architecture incorporates two Single-Pole Double-Throw (SPDT) switches positioned between the two DC power sources. These switches facilitate dynamic power management by enabling controllable power flow regulation between the DC supplies under varying demands, while concurrently providing electrical isolation for a faulty DC source in the event of a malfunction.
- Auxiliary Switches: Four auxiliary switches are integrated into the network to introduce additional degrees of freedom for reconfiguration. These devices enable rapid adaptation of the power routing under diverse operating conditions, thereby ensuring uninterrupted system operation.

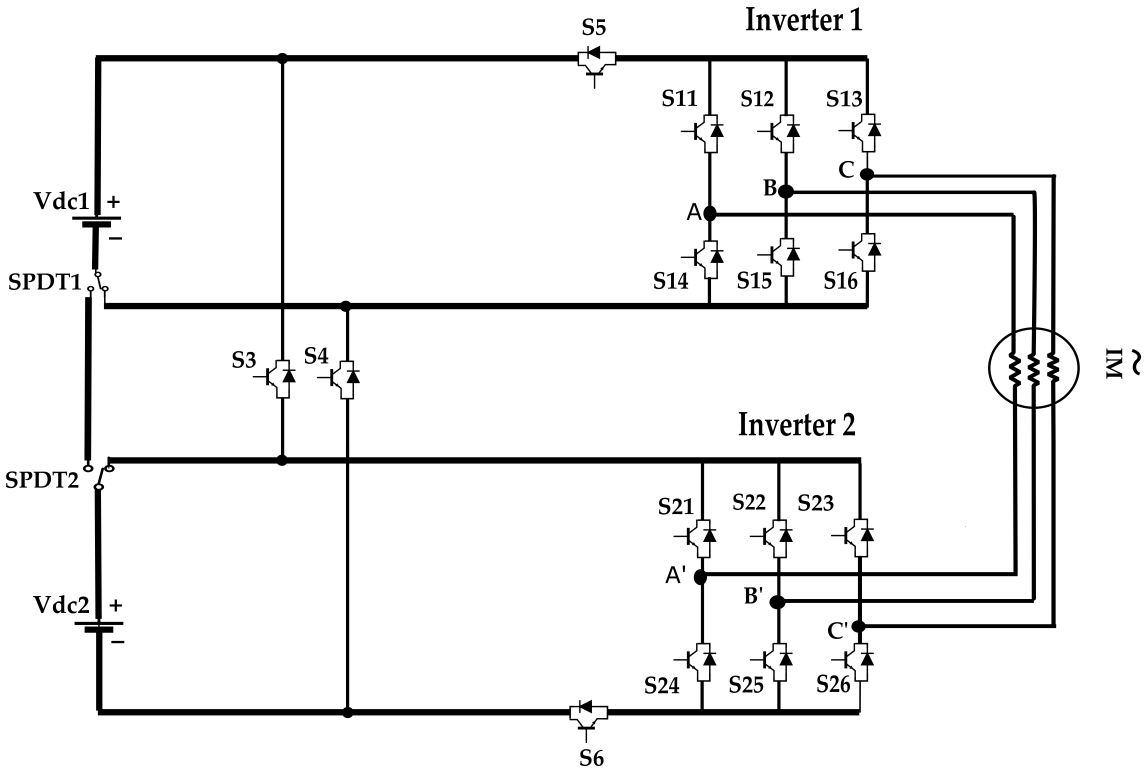


Figure 6. The proposed dynamic fault-tolerant topology for 3P-OEWIM.

3.3.1. Healthy Mode

Under healthy operating conditions, the proposed OEWIM architecture functions in its optimal state with all network components in their default configurations. The operational status of the system in this mode is defined as follows:

- Power Distribution: Each inverter is independently energized by its respective separate DC supply, thereby delivering balanced voltage and current profiles to the stator windings. The dual-inverter scheme operates symmetrically to satisfy the load demand while ensuring stable electromechanical performance.
- SPDT Switches: The SPDT switches remain in their default positions, establishing a direct connection between each DC supply and its corresponding inverter. This topology guarantees uninterrupted power transfer during conventional operation.
- Auxiliary Switches: The auxiliary switches S_3 and S_4 are set to their default open states, whereas S_5 and S_6 are maintained in their default closed states. This switching configuration preserves the standard power routing path, ensuring that S_3 and S_4 remain disengaged until a fault condition is detected.
- System Performance: The machine operates within a conventional OEW configuration fed by isolated DC sources, which inherently eliminates ZSC circulation and enables multilevel voltage waveform generation. This topology also accommodates hybrid energy storage integration, facilitating flexible power management between the independent DC sources while maintaining high efficiency and minimal switching losses.

3.3.2. Faulty Mode

The faulty mode operation is categorized into three main types: inverter faults, DC supply faults, and the simultaneous occurrence of both.

1. Inverter Faults:
Inverter faults are divided into two categories: faults from a single inverter and faults from both inverters.

a. Faults from a Single Inverter: Faults from a single inverter may occur at the switch level, manifesting as either open-circuit or short-circuit conditions. The core idea in correcting this fault is to form a neutral point using the faulty inverter and connect the two DC supplies in series, allowing the motor to revert to a conventional star configuration with its rated power.
To form the neutral point from the faulty inverter, the fault can be categorized into two types:

   i. Faults involving a single switch or multiple switches from the same level:
   For open-circuit faults affecting one or multiple switches at the same inverter level (e.g., the upper level), the remaining healthy switches of the same level are opened, while all three switches of the opposite level are closed to establish the neutral point.
   For short-circuit faults affecting one or multiple switches at the upper level, all remaining healthy switches of the same level are closed, while all three switches of the opposite level are opened to isolate the faulted branch and reconfigure the neutral point.
   To enable series connection of the two DC supplies, $SPDT_1$ and $SPDT_2$ switches are employed. In addition, two auxiliary switches are used to connect the remaining inverter to the DC supplies. This configuration enables the maintenance of rated power even under multiple switch fault conditions, including open- and short-circuit faults. For illustration, under an open-circuit fault affecting S_{21}, switches S_{24}, S_{25}, and S_{26} are closed to form the neutral point, while $SPDT_1$ and $SPDT_2$ are configured to connect the two DC supplies in series, as shown in Figure 7.
   When multiple switches at the same level fail under open-circuit conditions without simultaneous failure of all devices, an enhanced reconfiguration can be established, ensuring continued operation and extended fault tolerance to the second inverter. For example, if switches S_{21} and S_{22} fail while S_{23} remains operational, the switches associated with S_{21} and S_{22} (i.e., S_{24} and S_{25}) are turned ON, followed by the simultaneous closing of S_{23} and S_{26}, even though they belong to the same inverter leg. The risk of a DC supply short circuit is eliminated, as the corresponding DC source is disconnected from the faulty inverter and reconfigured in series with the second DC supply. In this case, switches S_3 and S_6 are used to control the neutral point, resulting in an equivalent (3 + 1)L-NAL configuration. The system then operates as a conventional star-connected IM with a controlled neutral point, ensuring continued operation under faults affecting the second inverter, as shown in Figure 8.

   ii. Switches Fail at Different Levels:
   When two or more switches at different inverter levels are affected by open- or short-circuit faults, the neutral point can still be established by reconfiguring a single inverter leg into a fully conducting state. For example, if S_{14}, S_{13}, and S_{12} are short-circuited, S_{11} and S_{15} are opened, while S_{16} is closed. This configuration forces one inverter leg into a fully conducting state, ensuring continued system operation and proper formation of the neutral point, as illustrated in Figure 9.
   In the case of open-circuit faults affecting two switches at different levels (one from the upper level and the other from the lower level), the corresponding switches within each affected leg are closed, while

all switches of the healthy leg are also closed to re-establish the neutral point and preserve the original star-connected operating mode with a controlled neutral connection. For example, if S_{11} and S_{15} become open-circuited, the corrective approach is to close S_{14} and S_{12}, as well as both S_{13} and S_{16}, to establish the neutral point. Additionally, $SPDT_1$ ensures the isolation of the faulty DC supply from the circuit, preventing short-circuit issues when two switches from the same leg are closed and ensuring the safe formation of the neutral point. The system now uses S_5 and S_4 to control the neutral point voltage as illustrated in Figures 9 and 10.

If two switches in the same inverter leg are affected by a short-circuit fault, the neutral point can still be established by utilizing the faulted leg as the neutral connection. This is achieved by isolating the affected leg from the DC supply using the corresponding SPDT switch and reconfiguring the remaining healthy legs.

The resulting configuration is equivalent to a star-connected IM with a controlled neutral point, as illustrated in Figure 10, while maintaining rated power operation.

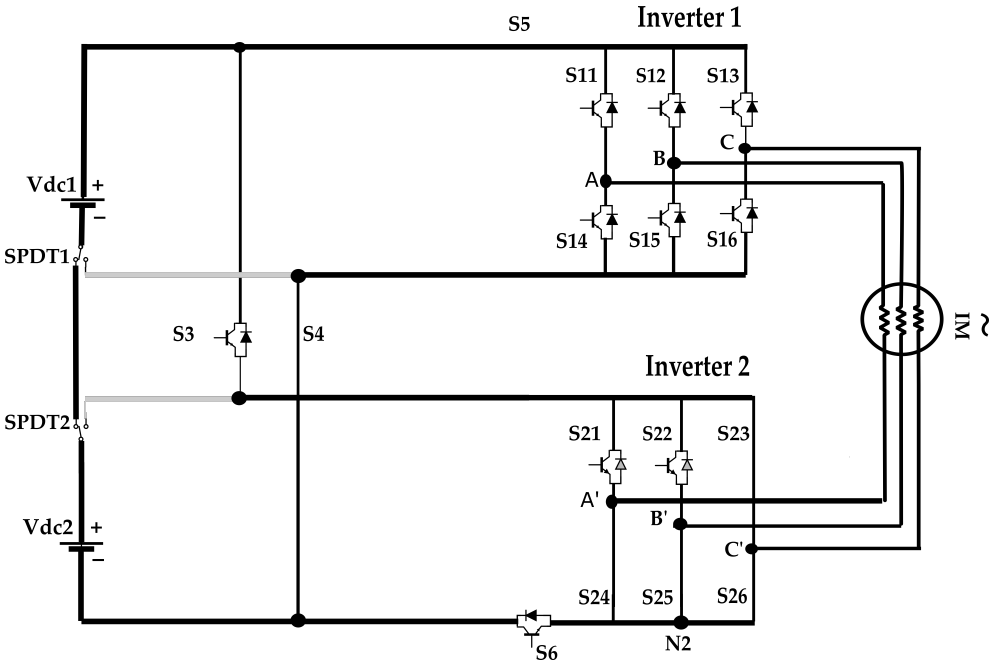


Figure 7. Open-circuit fault in two switches at the same level of a single inverter.

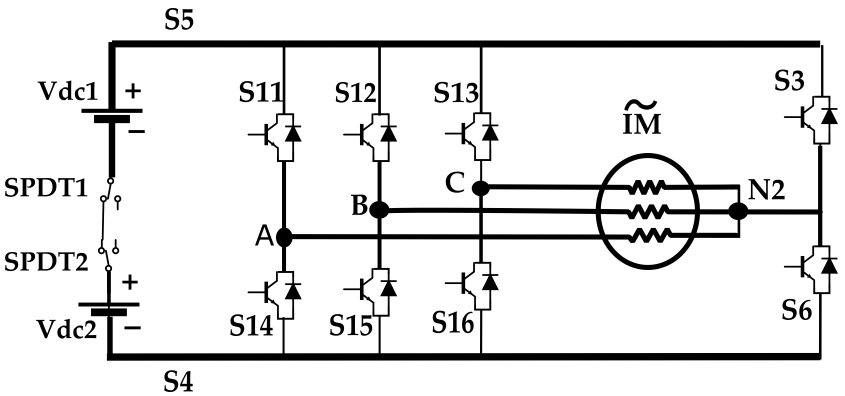


Figure 8. Equivalent star configuration under open-circuit fault in two switches at the same level.

In these cases, the system is reconfigured into a conventional three-phase star-connected two-level inverter structure, where the SVPWM strategy is adapted from a three-level to a two-level modulation scheme. This reconfiguration is achieved while maintaining rated power operation, as the two DC supplies are connected in series, ensuring the preservation of both rated voltage and current levels. The faulty inverter is short-circuited and clamped, while the healthy inverter supplies the required output voltage. In this configuration, the SVPWM hexagon maintains the same size as the larger hexagon associated with the three-level operating mode.

b. Faults from both inverters:

If faults occur in both inverters, the neutral point can still be established by applying the same FT strategies described previously. When a fault occurs in one inverter, the system reconfigures to form the neutral point, which is then connected to an alternative leg and operated under a new FTC strategy, while maintaining the capability to accommodate subsequent faults in the second inverter. In certain scenarios, the system may be required to transition to a two-phase operating mode. In this case, the IM operates as a two-phase machine, utilizing only two healthy phases to preserve functionality while maintaining fault tolerance.

In the two-phase mode, there are two possible configurations:

i. Conventional Star IM with Controlled Neutral Point.
ii. OEWIM Two-Phase Motor.

The first configuration, a conventional star IM with a controlled neutral point, is shown in Figures 11 and 12. This setup allows the motor to operate efficiently in two-phase mode while maintaining control over the neutral point for enhanced FT.

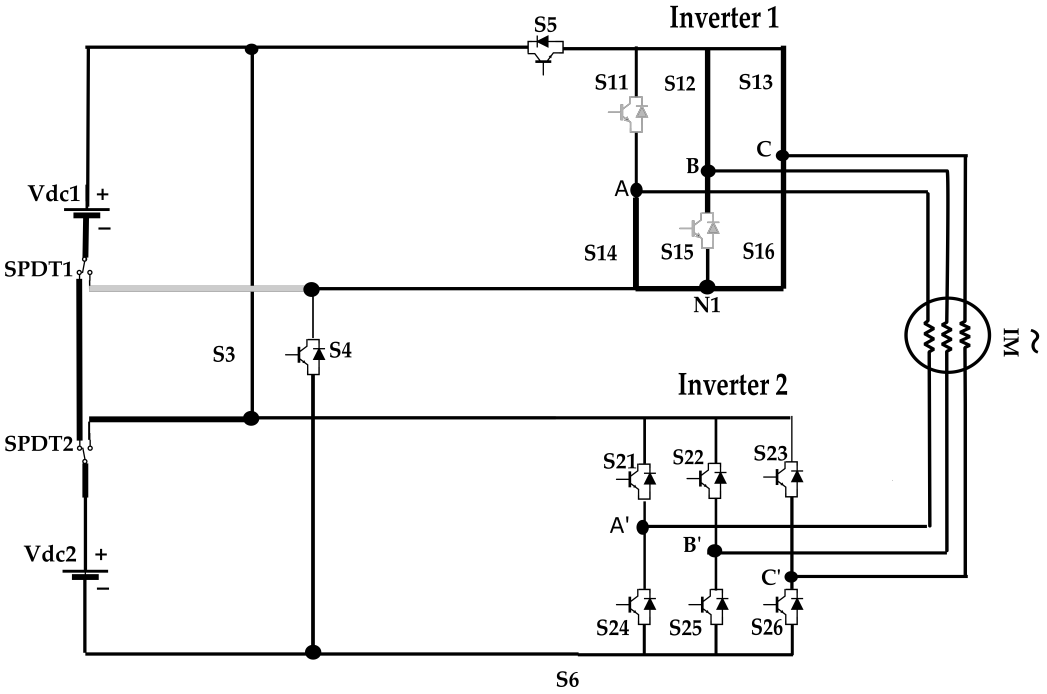


Figure 9. Open-circuit fault in two switches at different levels of a single inverter.

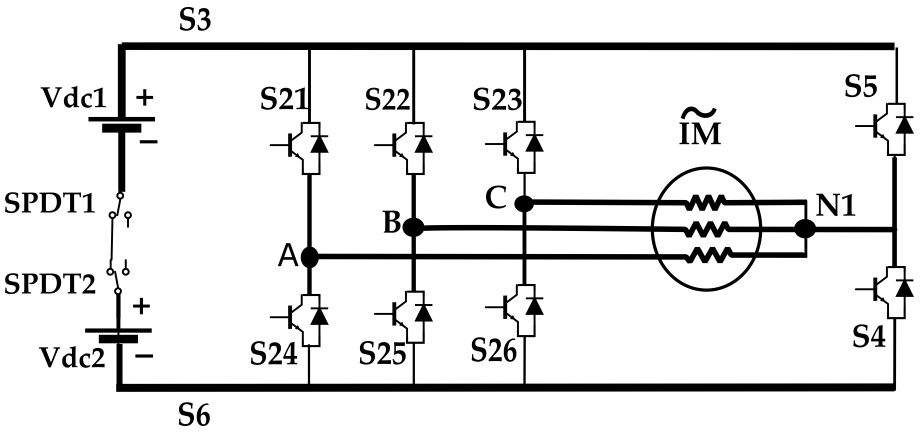


Figure 10. FT configuration when two switches from different levels fail.

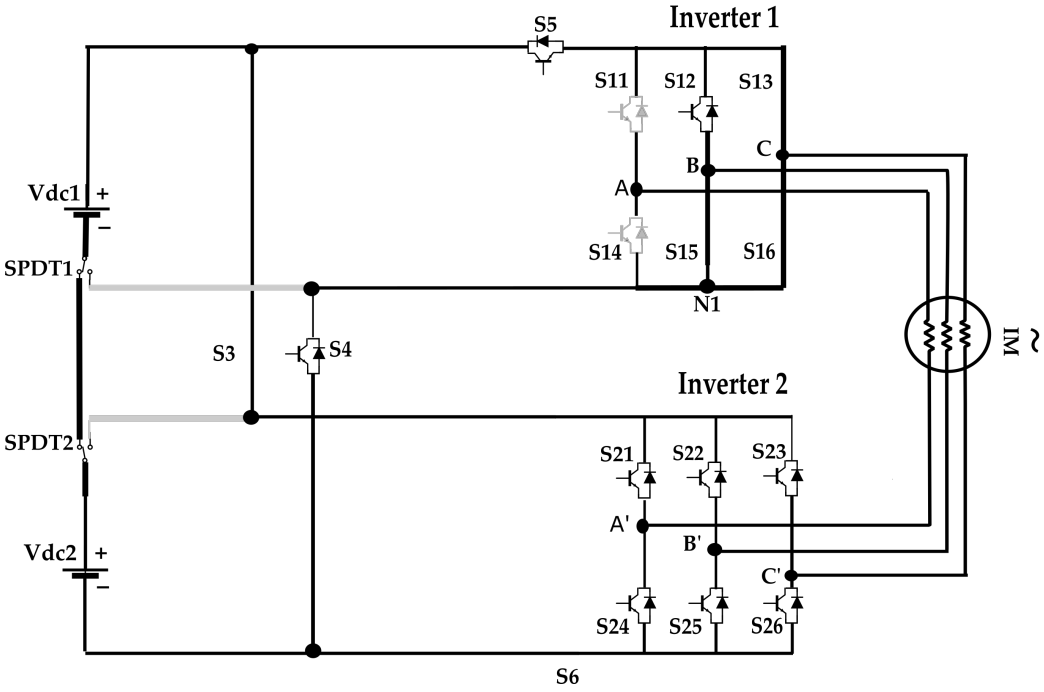


Figure 11. Open-circuit fault in both switches of the same leg in a single inverter.

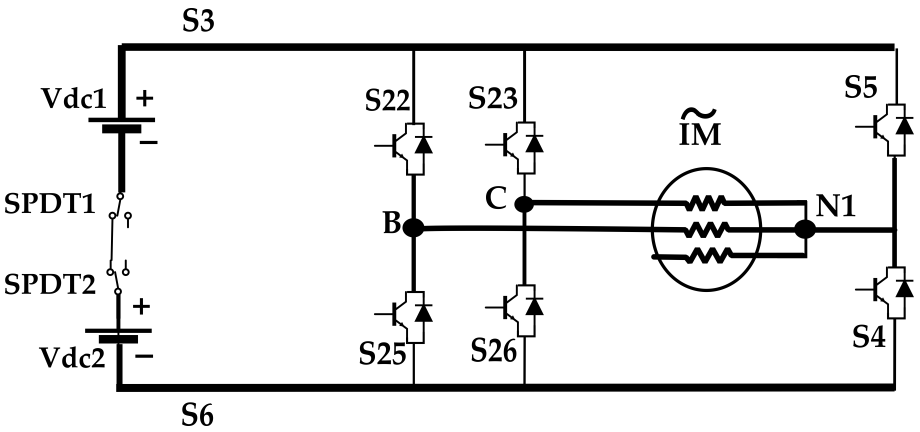


Figure 12. Equivalent star configuration under open-circuit fault in both switches of the same leg.

In the OEW two-phase configuration, there are two possible setups:

i. With Two DC Supplies in Parallel: This configuration connects the DC supplies in parallel to provide a balanced power distribution to the two-phase system, as presented in [66] and shown in Figures 13 and 14.

ii. With a Common DC Supply: This setup connects both inverters to a single DC supply, providing a ZSC path, as illustrated in Figure 15.

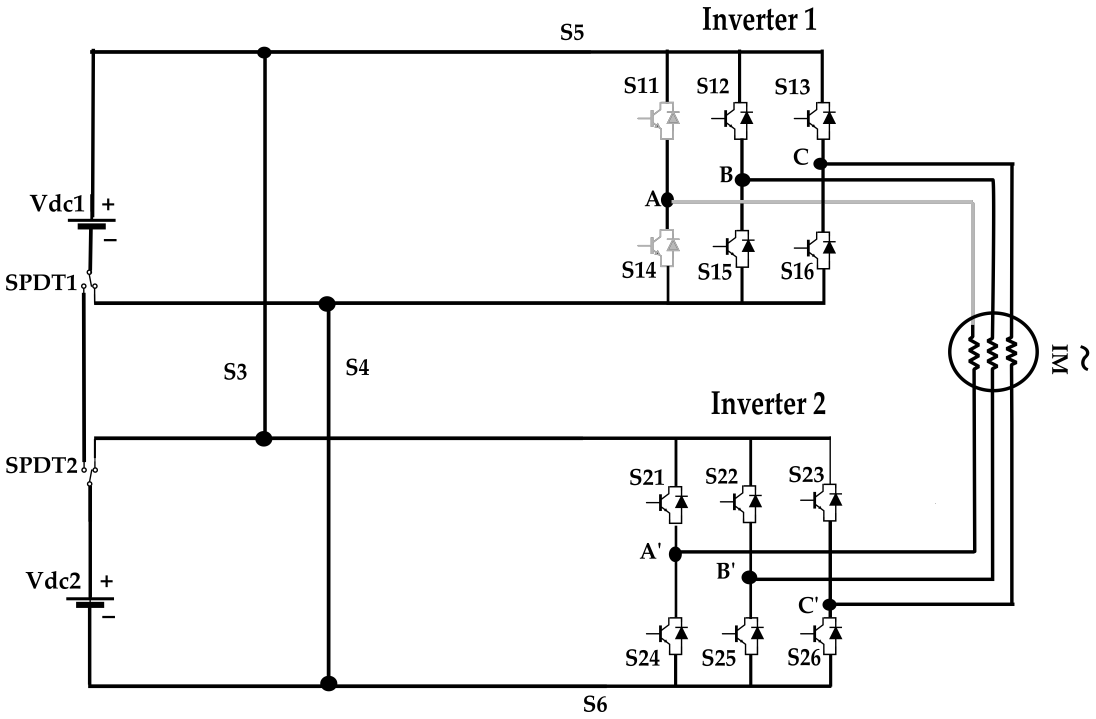


Figure 13. OEWIM two-phase operation mode with two DC supplies connected in parallel.

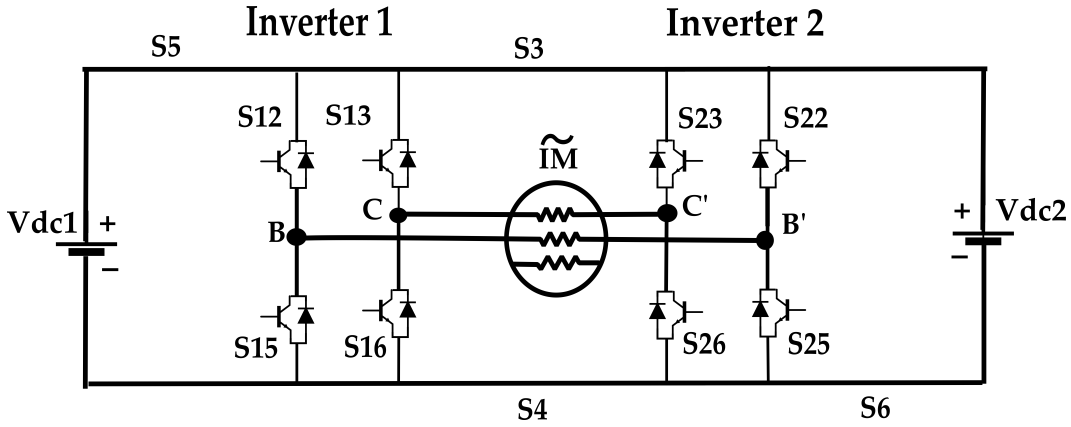


Figure 14. OEWIM two-phase operation mode with a common DC supply.

In summary, the proposed FTC strategy addresses inverter faults by organizing the reconfigured operating modes based on fault severity as follows:

- Maintaining the Three-Phase System with Rated Power: The system remains in three-phase operation with a new FT configuration, ready to handle additional faults.
- Transitioning to Two-Phase Mode: This occurs in specific cases, such as:
  - Two open-circuit switches from the same leg.
  - An open-phase fault, where one phase becomes completely disconnected.

In certain cases, such as an open-circuit switch in the remaining inverter as a second fault, the system can alternate between three-phase and two-phase operation [14].

In the two-phase mode, there are three possible FT configurations: Two configurations in OEW configurations, and one in the normal star configuration.

2. DC Supply Faults:

In the case of a DC supply failure, the OEW configuration can be maintained by reconfiguring the DC-link structure through SPDT switches. The faulty DC source is isolated, while the corresponding inverter is reconnected to the healthy DC supply to preserve system operation.

For example, if DC_2 fails, it is disconnected using $SPDT_2$. Subsequently, auxiliary switches S_3 and S_4 are closed to connect Inverter 2 to DC_1, ensuring continuity of the three-level OEW operation, as illustrated in Figure 15.

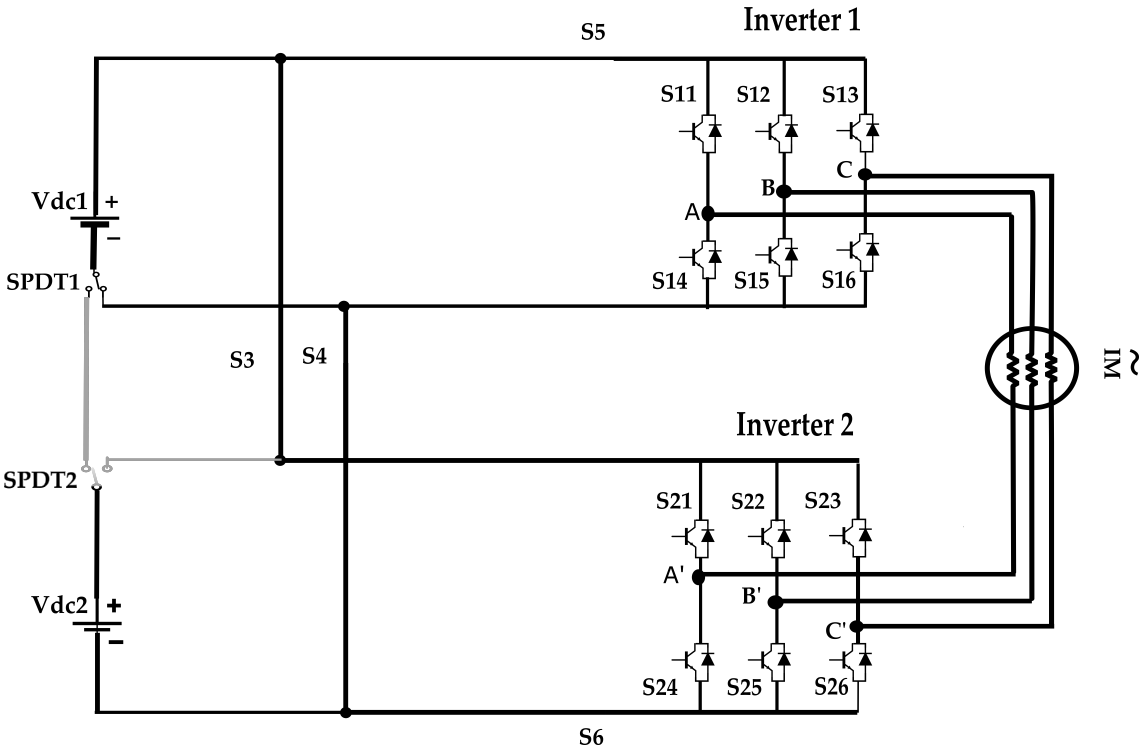


Figure 15. FT configuration for a DC supply fault.

This configuration corresponds to the OEW topology with a common DC supply. In this case, the voltage amplitude is inherently limited by the single available DC source; however, the three-level voltage waveform characteristics are preserved. Unlike the isolated configuration, the common DC bus creates a closed loop for ZSC, enabling fault operation without the need for a controlled neutral-point bridge. This inherent current path enhances the capability of the system to tolerate additional faults.

3. Both DC + Inverter Faults:

The fault can affect the DC supply along with either one inverter or both inverters.

a. Fault in One DC Supply and One Inverter: In the case of a fault in one DC supply and one inverter, they can either be from the same side or from different sides.

i. DC Supply and Inverter Fault on the Same Side:

When the faulty inverter corresponds to the faulty DC supply, the system maintains operation by isolating the faulty DC source using $SPDT_1$ while reconfiguring the remaining healthy switching devices to establish

the neutral point. In this case, the system operates as a star-connected IM with reduced power capability, while maintaining fault tolerance against additional disturbances in the remaining inverter. For instance, if DC_1 fails and switches S_{11} and S_{15} are open-circuited, $SPDT_1$ isolates DC_1, while S_{12}, S_{13}, S_{14}, and S_{16} are configured to form the neutral point. Auxiliary switches S_3, S_4, and S_5 are then used to realize a controlled neutral-point connection, resulting in the configuration shown in Figures 16 and 17.

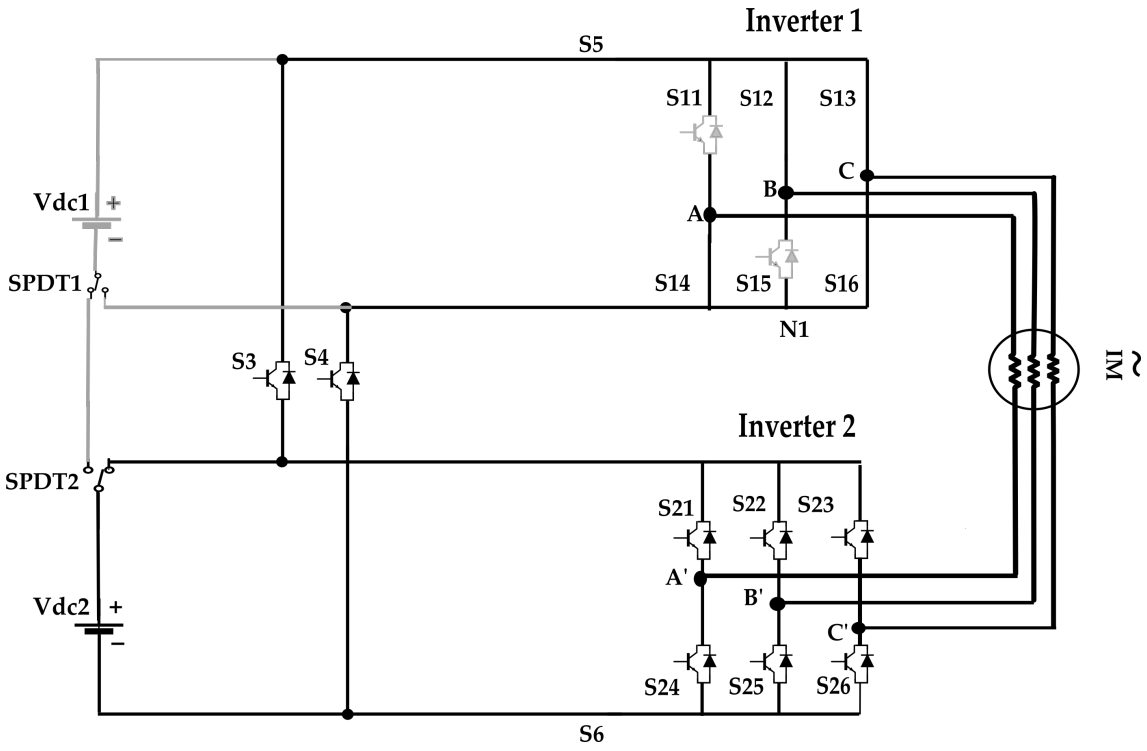


Figure 16. DC supply failure with two open-circuit switches on the same side.

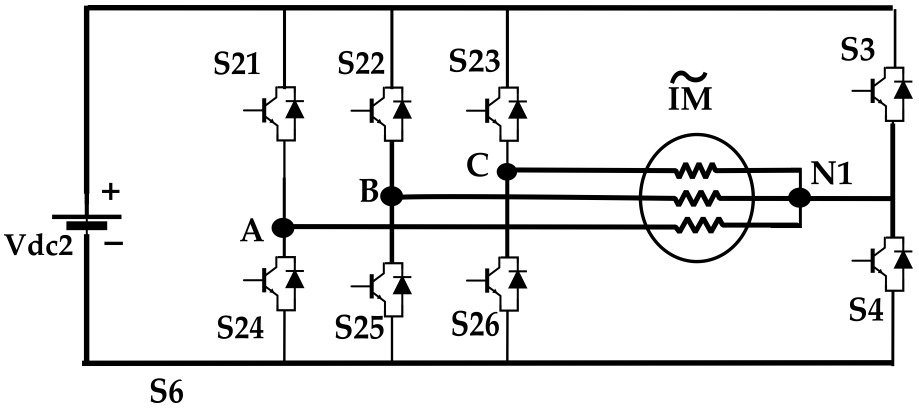


Figure 17. DC supply failure with two open-circuit switches on the same side.

ii. DC Supply and Inverter Fault on Different Sides:
When the faulty DC supply and the faulty inverter are located on different sides, the healthy DC supply can be connected to the healthy inverter, while both faulty units are isolated. The neutral point is then established using the remaining healthy switching devices, enabling continued operation under degraded conditions. For example, if DC_1 fails and an open-circuit fault occurs in S_{21}, $SPDT_1$ isolates DC_1, while

S_{24}, S_{25}, and S_{26} are used to form the neutral point. In addition, S_3 and S_4 connect Inverter 1 to DC_2. The neutral point can be further controlled by connecting it to the DC bus through S_6, while an additional healthy switch such as S_{23} is used to stabilize the voltage levels, as illustrated in Figures 18 and 19.

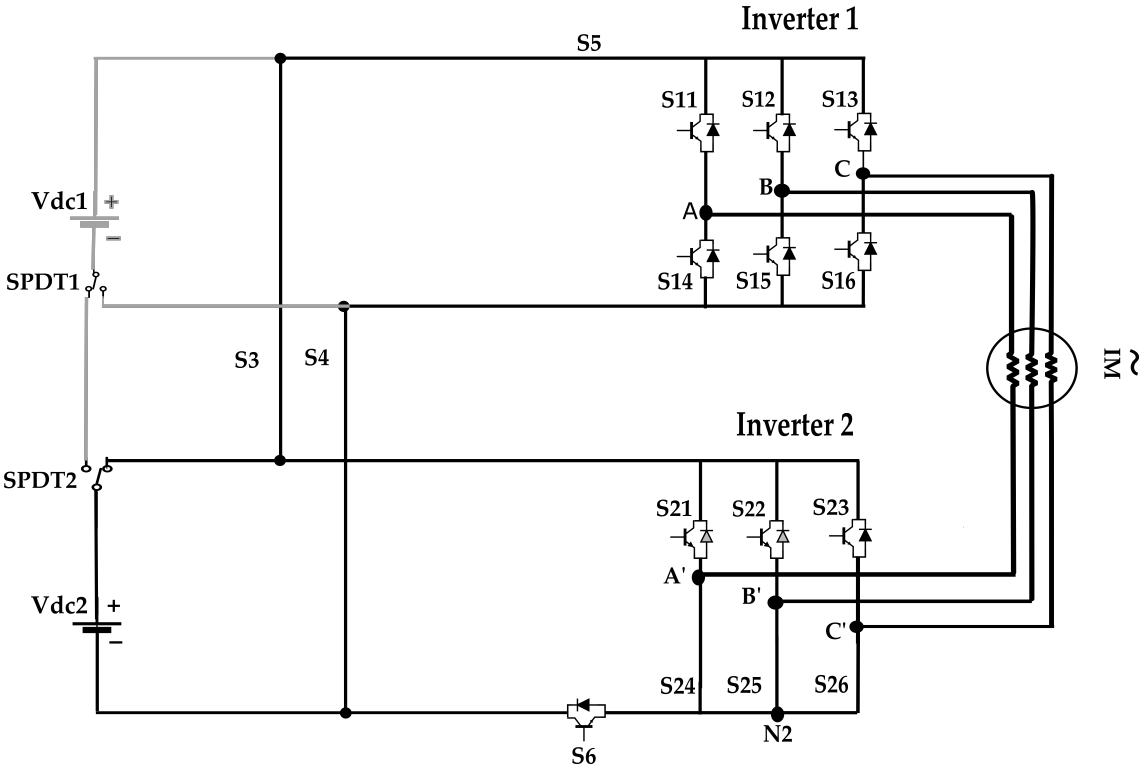


Figure 18. DC supply failure with two open-circuit switches on different sides.

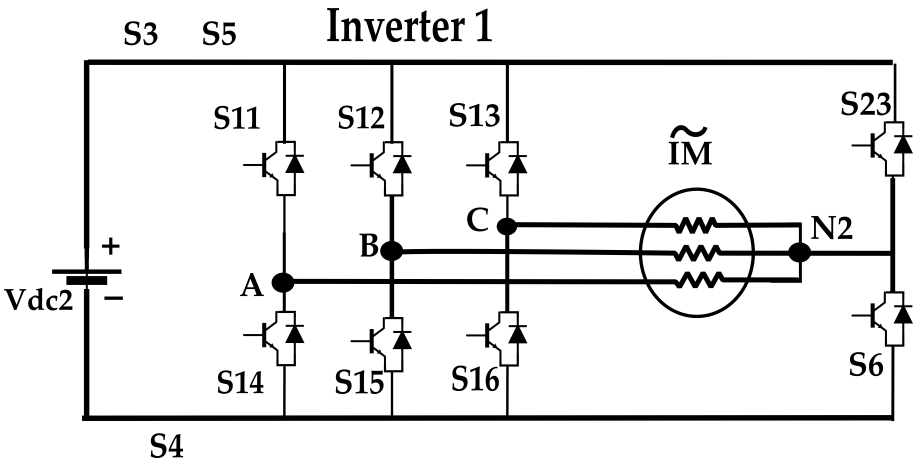


Figure 19. DC supply failure with two open-circuit switches on different sides.

b. Fault in One DC Supply and Both Inverters: In the case of a fault involving one DC supply and both inverters, two alternative FT reconfiguration strategies can be applied.

   i. Two-Phase Star Motor Mode: A controlled neutral point is established using the available inverter states, enabling a ZSC path, allowing the system to continue operating with a single inverter in two-phase mode or both two and three phases mode [14], as shown in Figure 20.

ii. Two-Phase OEW with a Common DC Supply: The system is reconfigured by connecting both inverters to a common DC supply, provided that the affected switching states correspond to compatible windings. This configuration enables OEW operation with a natural ZSC path and ensures the generation of an RMMF under two-phase operation, as shown in Figures 21 and 22.

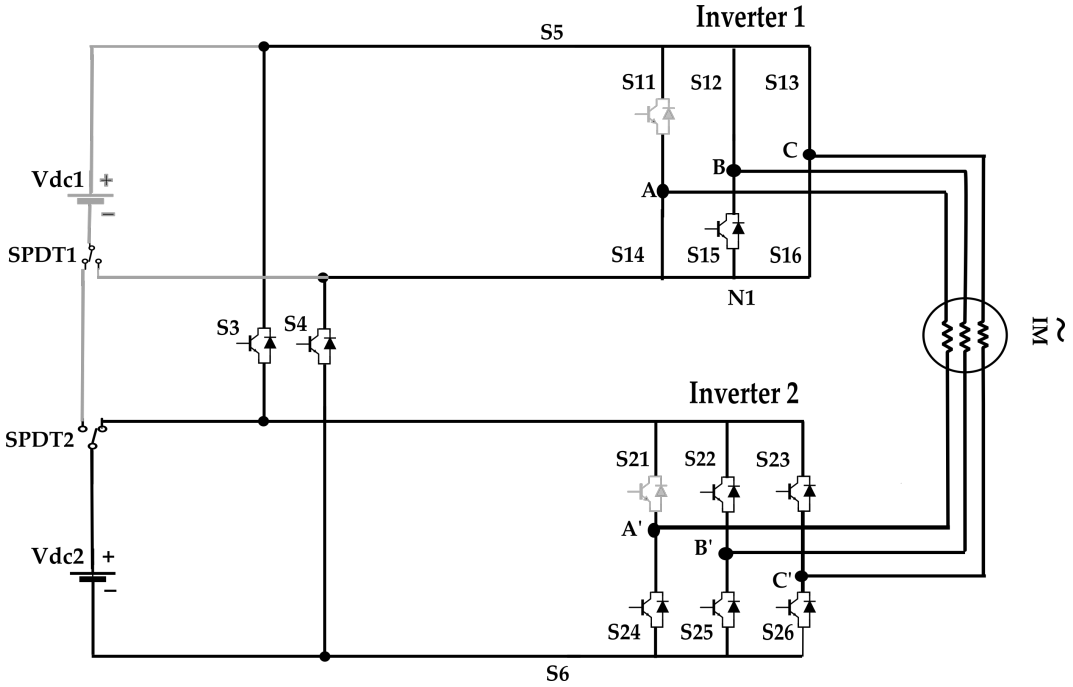


Figure 20. DC supply failure with two open-circuit switches from both inverters.

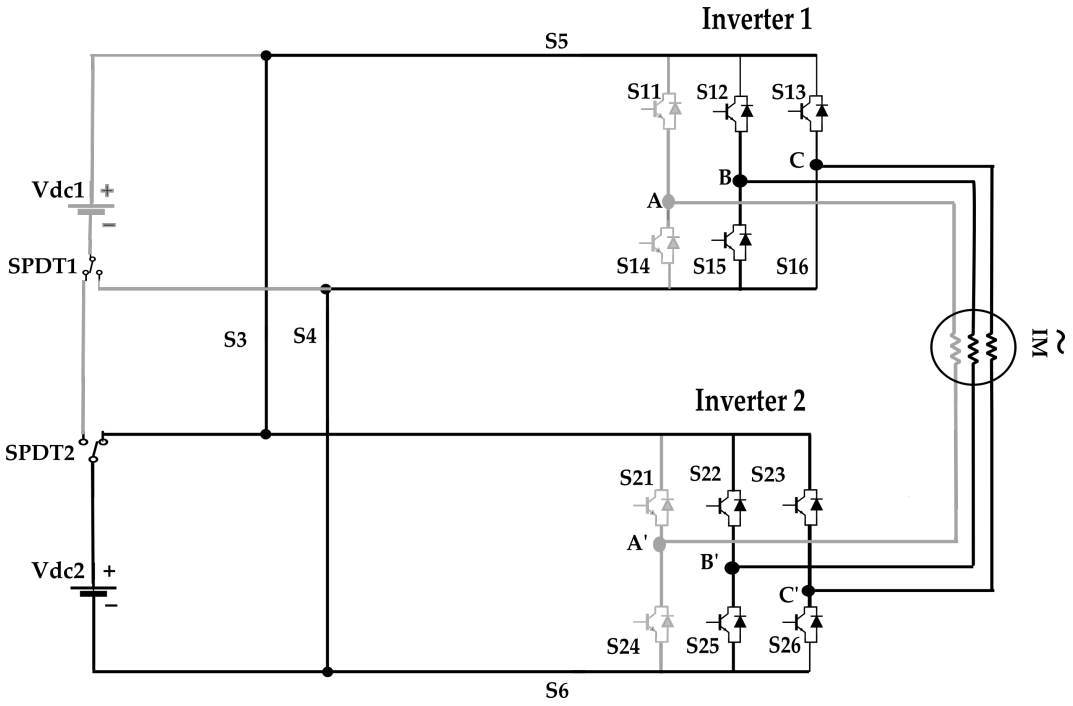


Figure 21. OEW common DC supply FTC for a DC supply failure with two open-circuit switches from both inverters.

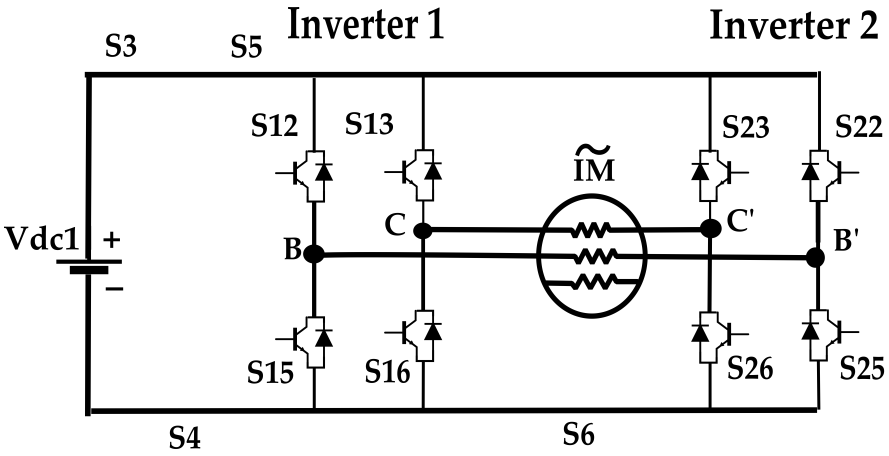


Figure 22. OEW common DC supply FTC for a DC supply failure with two open-circuit switches from both inverters.

3.4. Comparison with Existing Topologies

To evaluate the proposed dynamic topology, Table 1 compares its main features and limitations with existing fault-tolerant configurations reported in the literature. Existing topologies are typically designed for a single, specific failure mode, and their hardware arrangements cannot adapt to consecutive faults or multi-component failures. In addition, conventional strategies often suffer from over-isolation, where isolating a damaged converter needlessly disables healthy energy sources or forces healthy machine phases out of service. The proposed architecture resolves these limitations using an auxiliary network consisting of four bidirectional switches and two SPDT contactors. This setup enables independent reconfiguration of both the DC sources and the inverter legs, establishing a flexible platform that maintains operation across complex failure scenarios.

In conventional separate-DC OEW drives, fault tolerance typically relies on passive neutral clamping by switching all upper or all lower devices of the faulty inverter. However, this classical mechanism fails completely under mixed-level switch faults (such as an open upper switch in one leg and an open lower switch in another) or under leg shoot-through short circuits, where a standard zero-vector cannot be synthesized. Furthermore, because each DC supply is permanently tied to one inverter, isolating the damaged inverter inevitably cuts off its associated DC source, reducing the available power to 50%. In contrast, the proposed topology uses the auxiliary switches to form a controlled neutral connection regardless of whether the fault affects upper, lower, or mixed switches. Even under severe conditions such as a leg shoot-through, which normally causes an immediate DC-link short circuit and drive shutdown, the faulted leg is isolated from the DC bus and repurposed as an active neutral path. Simultaneously, the two isolated DC supplies are connected in series, preserving full rated line voltage and enabling the surviving healthy inverter to deliver 100% of the rated power (P_n) in symmetrical three-phase star mode.

The proposed architecture also combines the operational advantages of common-DC and separate-DC configurations while avoiding their respective drawbacks. Under healthy conditions, the drive operates with isolated DC supplies to eliminate circulating zero-sequence currents, synthesize three-level voltages, and avoid bulky common-mode filters. If a single DC supply experiences an outage while both inverters remain healthy, the auxiliary network dynamically connects both inverters to the surviving DC source in parallel. This preserves three-level OEW operation, avoiding immediate degradation into a single-inverter star mode. More importantly, when an inverter fault on one side coincides with a DC source failure on the opposite side of the machine, cross-terminal routing dynamically pairs the surviving healthy inverter with the surviving DC supply,

maintaining balanced three-phase operation where conventional systems suffer complete drive shutdown.

Table 1. Comparison of state-of-the-art fault-tolerant topologies with the proposed dynamic architecture.

Topology Category	References	Targeted Fault(s)	Post-Fault Power	Phase Mode	Key Features & Main Limitations
(3 + 1)L-NAL Star (Controlled Neutral Point)	[8,10,11,15–17,72]	Open-switch or open-phase fault (including two open switches in the same leg)	57.7% (thermal limit)	2-phase asymmetrical	Features: Single DC source; controlled 4th leg provides active neutral regulation to reduce torque ripples; supports hybrid 3-phase/2-phase post-fault operation. Limitations: Not an OEW configuration (lacks multilevel voltage synthesis, higher voltage utilization, and hybrid storage); requires a 4th inverter leg with neutral TRIACs; no DC supply fault tolerance; no capacity for consecutive compound faults.
OEWIM Common DC (Natural ZSC Path)	[7,50,61–63,65,73]	Open-switch or open-phase fault (including two open switches in the same leg)	50–70.7%	Hybrid 3-phase/2-phase or 2-phase asymmetrical	Features: Single DC source; natural ZSC path enables post-fault current return without auxiliary switching devices. Limitations: Requires continuous active ZSC suppression during healthy operation; no tolerance to switch short circuits; no DC supply redundancy; no capacity for consecutive compound faults.
OEWIM Separate DC (Neutral-Point Clamping)	[66,67,69,70,74]	Open-switch, short-circuit switch, or single DC supply fault	50%	3-phase symmetrical star	Features: Inherent ZSC-free operation; enables higher multilevel voltage synthesis via asymmetric DC ratios; supports hybrid energy storage integration. Limitations: Isolating faulty inverter permanently disconnects its DC source; neutral clamping fails under mixed-level switch faults; total shutdown under cross-terminal faults; lacks a ZSC path for open-phase; no capacity for consecutive compound faults.
OEWIM Parallel DC (Two-Phase Mode)	[66,75]	Open-switch or open-phase fault (including two open switches in the same leg)	57.7% (thermal limit)	2-phase asymmetrical (Dual H-Bridge)	Features: OEW multilevel voltage synthesis; parallel DC connection enables two-phase dual H-bridge operation under open-switch or open-phase faults. Limitations: Restricted to degraded two-phase mode under inverter faults; cannot form a neutral point for symmetrical star operation; no tolerance to switch short circuits; no capacity for consecutive compound faults.
Proposed Dynamic Architecture (This Work)	Case 1: Single Inverter Fault	Single or multiple switch faults (open/short circuit, mixed levels, or leg shoot-through) in one inverter	100% (full rated)	3-phase symmetrical star	1. Integrated features: Combines separate-DC advantages (ZSC-free operation, multilevel voltage, and hybrid storage), common-DC natural ZSC path for open-phase faults, and star drive neutral-point control. 2. Avoids over-isolation: Under inverter faults, preserves symmetrical 3-phase star with full rated power by connecting DC sources in series instead of forcing degraded two-phase mode or losing half the DC-link voltage; under DC supply faults, isolates only the faulty DC source without disabling its inverter, keeping OEW dual-inverter operation. 3. Fault isolation in complex scenarios: Forms controlled neutral point under mixed upper and lower switch faults; repurposes shorted legs as active neutral paths; resolves cross-terminal faults by connecting surviving DC supply to surviving inverter. 4. Diverse and consecutive fault tolerance: Handles switch open/short circuits, open phases, and DC source failures; tolerates consecutive multi-stage faults across both inverters and DC supplies; four-tier power degradation. Limitations: Requires auxiliary hardware components (4 bidirectional switches and 2 SPDT contactors).
	Case 2: Stator Phase Loss	Open-phase loss of one stator winding, or switch faults affecting both sides of one phase	57.7% (thermal limit)	2-phase asymmetrical	
	Case 3: Inverter Fault + DC Outage	Combined failure: Inverter switch failure together with single DC supply outage (on same or opposite sides)	50%	3-phase symmetrical star	
	Case 4: Consecutive DC and Phase Faults	Consecutive compound failure: Single DC supply outage combined with stator phase loss (or open leg)	28.9% (thermal limit)	2-phase asymmetrical	

This reconfiguration capability establishes a four-tier power degradation structure: transitioning from full rated power (100%P_n) in three-phase series-DC mode, to 57.7%P_n under an open-phase condition, 50%P_n under a single-DC source outage, and down to 28.9%P_n

during combined DC and stator phase loss. Instead of shutting down under compound or cascading failures, the drive maintains continuous rotation for critical limp-home operation. Furthermore, because the reconfigured drive physically operates within these established sub-topologies, advanced modulation and control strategies developed in the literature for separate-DC, common-DC, and star-connected drives can be directly applied to the corresponding operational state without requiring dedicated controller redesign.

4. Results and Discussion

As summarized in Table 1, the proposed architecture integrates several fault-tolerant configurations that have been individually established in the literature. Therefore, the analysis in this section focuses on evaluating the capability of the proposed dynamic topology to manage diverse and consecutive faults, isolate faulty components, and maintain stable operation across multi-stage failure sequences.

To evaluate this capability, several fault scenarios are investigated, covering sequential and compound failures affecting both inverters and the DC supplies. In addition, dynamic speed variations and mechanical load transitions are evaluated to examine post-fault performance under varying operating conditions. The dynamic response is analyzed across all operational phases: pre-fault steady state, the fault transient, and post-reconfiguration recovery. The nominal parameters of the simulated induction motor are provided in Appendix A (Table A1).

In all evaluated scenarios, the activation of the corresponding FT reconfiguration is intentionally delayed after each fault. This delay creates a worst-case test condition by allowing post-fault instability, including speed drops, torque pulsations, and current surges, before recovery is initiated. It also shows that the proposed dynamic topology can operate as an independent hardware reconfiguration layer that can be combined with different FDI algorithms, even when the diagnostic response is delayed.

4.1. Switches Failing at Different Levels (Upper and Lower)

This scenario investigates the FT operation of an OEWIM under two simultaneous open-circuit faults: switch S_{11}, corresponding to an upper switch in one leg, and switch S_{15}, corresponding to a lower switch in another leg. This condition is difficult because the faulty side cannot form a neutral point by fully short-circuiting the three motor phases through either the upper or the lower switch group.

Before the fault, the motor operated steadily at 1371 rpm with a light load torque of $T_L = 3.2\ \mathrm{N \cdot m}$ (approx. 14.5% of the rated torque $T_n = 22.0\ \mathrm{N \cdot m}$) and a balanced three-level voltage. The simultaneous faults produced a 600% current surge, voltage distortion, a large speed drop with oscillations, bidirectional speed fluctuations, and pronounced torque pulsations.

After activating the FT mechanism, the system recovered stable operation. The electromagnetic torque returned to its pre-fault load level ($3.2\ \mathrm{N \cdot m}$), while the speed recovered to 1368 rpm, slightly below the reference value due to motor slip. The current and voltage waveforms also stabilized. The post-fault voltage changed from a three-level waveform to a two-level waveform while preserving the rated voltage.

The FT strategy isolated the faulty switches and connected DC_1 of the faulty Inverter 1 in series with the second DC supply. This reconfiguration enabled neutral-point formation despite the simultaneous upper- and lower-switch faults. As a result, the system returned to a star configuration, preserved full rated power capability ($100\%P_n$), and restored motor operation close to the pre-fault condition. The corresponding simulation results are presented in Figures 23–26.

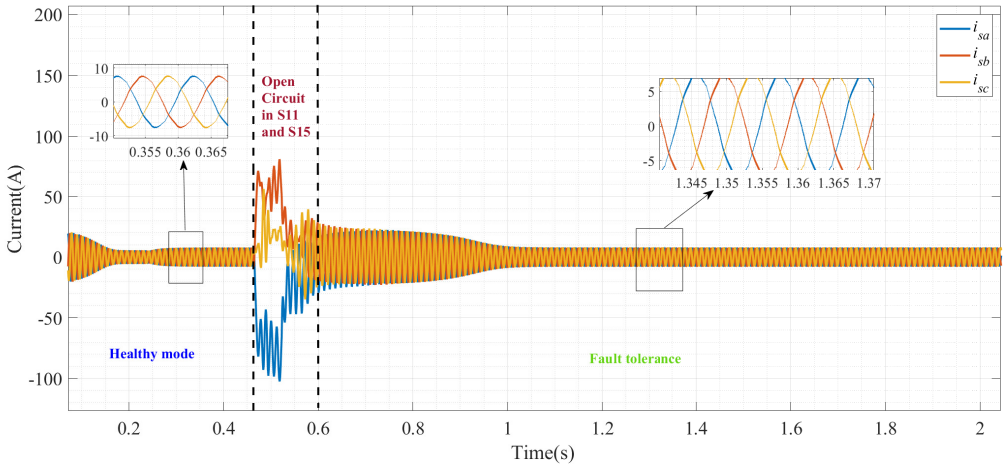


Figure 23. Stator current waveform under fault condition with switches failing at different levels.

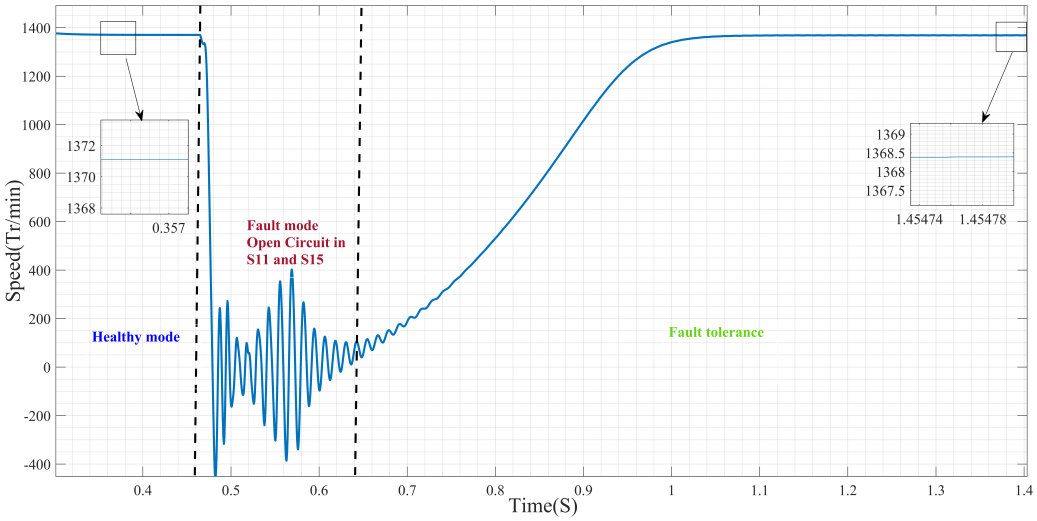


Figure 24. Rotor speed response under fault condition with switches failing at different levels.

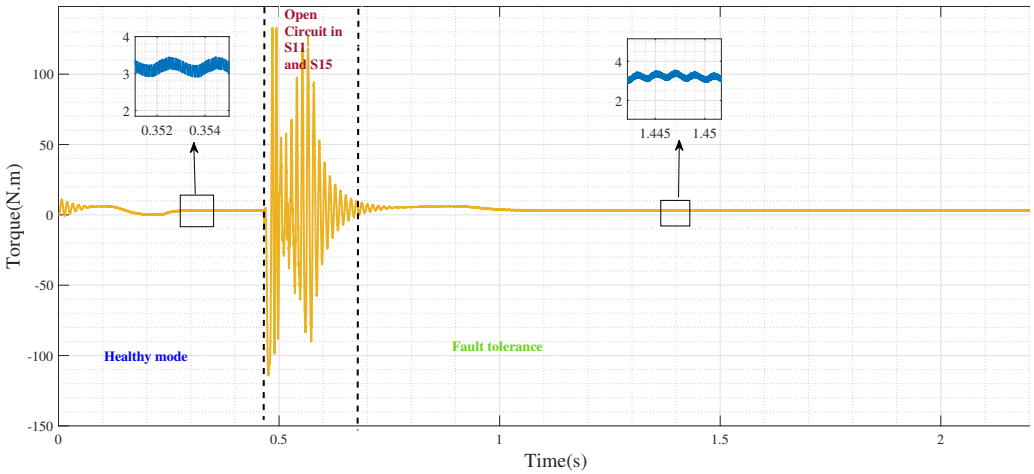


Figure 25. Electromagnetic torque response under fault condition with switches failing at different levels.

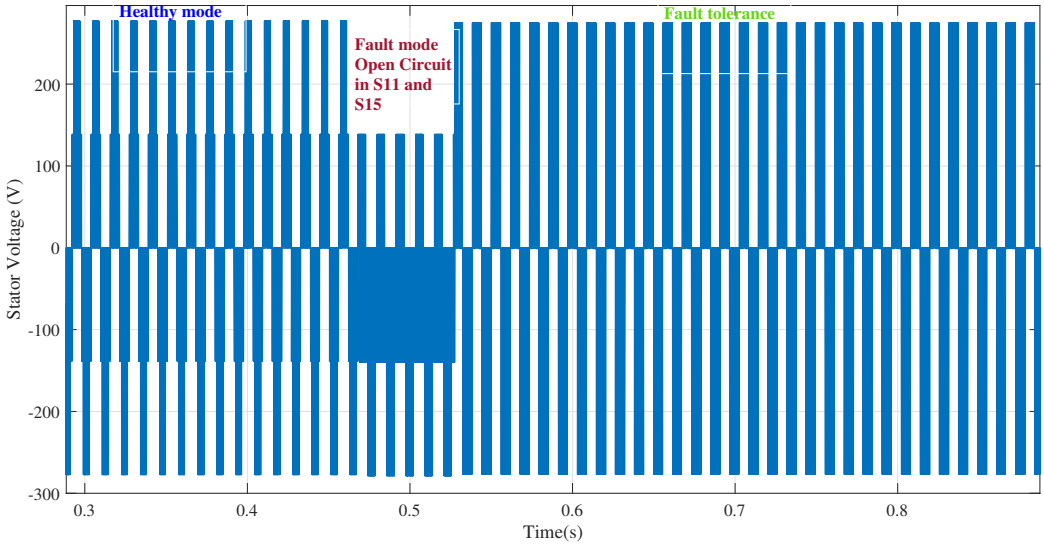


Figure 26. Stator voltage waveform under fault condition with switches failing at different levels.

4.2. DC Supply and Inverter Fault on Different Sides

This scenario investigates the FT operation of an OEWIM under a dual-fault condition involving a DC supply and an inverter on opposite sides of the drive. The first fault is a failure of DC_1, followed by an open-switch fault in Inverter 2.

Initially, the motor operates under no-load condition ($T_L = 0$ N · m). The speed is regulated at 1497.7 rpm, the torque remains at 0 N · m, and the currents are balanced and sinusoidal with a healthy three-level voltage waveform.

At $t = 0.5$ s, DC_1 fails. The speed begins to fluctuate, and the electromagnetic torque exhibits a ripple of approximately 2 N · m, ranging from about -1 N · m to $+1$ N · m. The phase currents also become distorted because of the unbalanced supply condition.

At $t = 0.8$ s, the first FT mechanism is activated. The system is reconfigured into a common DC bus topology by connecting the healthy inverter to the remaining healthy DC supply. This reconfiguration suppresses the torque oscillations and restores stable operation. The speed shows a slight reduction because of the voltage limitation imposed by the single DC source.

The second fault occurs at $t = 1.5$ s as an open-switch fault in Inverter 2. This fault causes a substantial loss of control, with a large speed drop, torque pulsations reaching approximately 8 N · m, and severe distortion and asymmetry in the three-phase currents.

At $t = 1.7$ s, the second FT mechanism is activated. The faulty Inverter 2 is isolated, and a neutral point is formed at the motor terminals, which transfers the drive to a star-connected single-inverter configuration. In this mode, the healthy Inverter 1 is supplied by DC_2. After the transition, the speed recovers close to the reference value, the torque returns to the pre-fault no-load condition (0 N · m), and the currents regain a balanced sinusoidal form. The corresponding simulation results are presented in Figures 27–30.

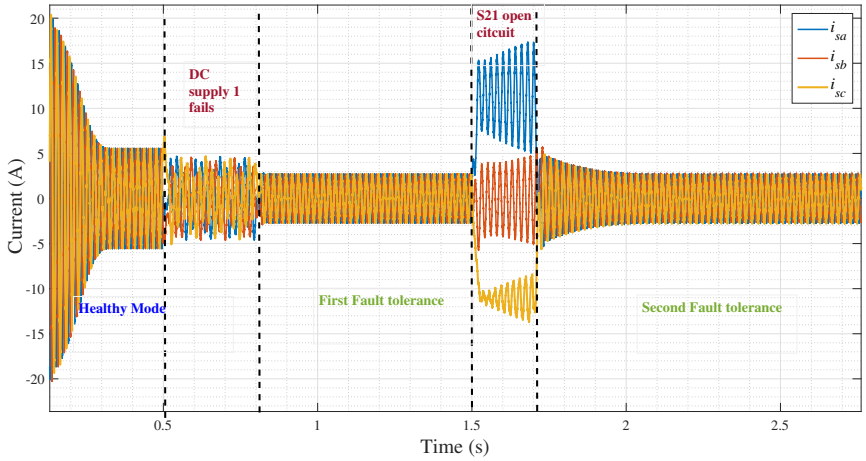


Figure 27. Stator current waveform under a DC supply fault and inverter fault occurring on opposite sides.

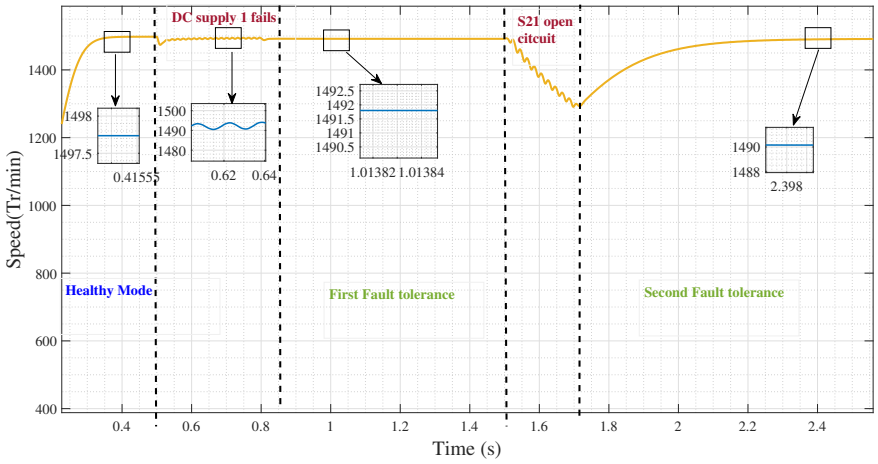


Figure 28. Rotor speed response under a DC supply fault and inverter fault occurring on opposite sides.

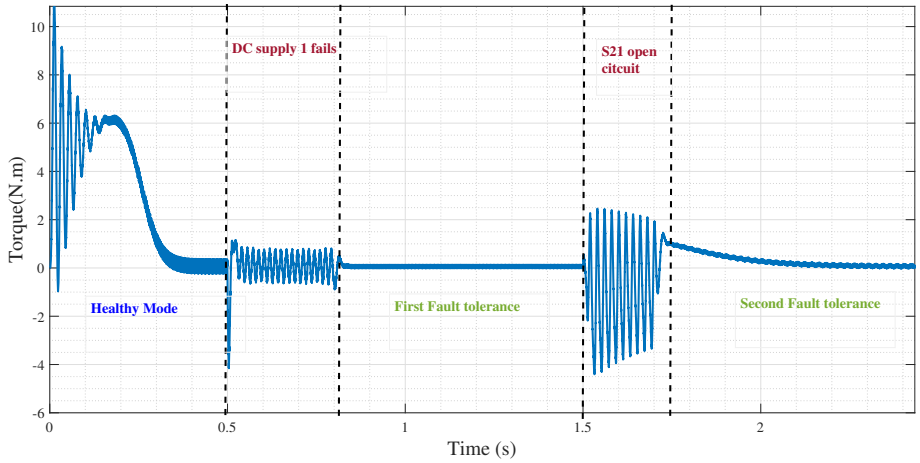


Figure 29. Electromagnetic torque response under a DC supply fault and inverter fault occurring on opposite sides.

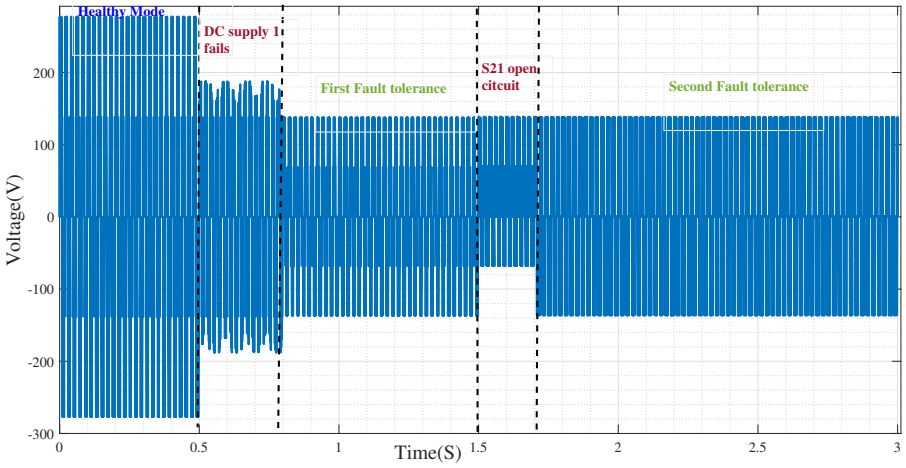


Figure 30. Stator voltage waveform under a DC supply fault and inverter fault occurring on opposite sides.

4.3. DC Supply Fault Combined with Faults in Both Inverters

The FT operation of the OEWIM is evaluated under a compound fault scenario involving three failures: a short circuit of two switches in the same leg of Inverter 1, the failure of DC_1, and an open-circuit fault in a switch of Inverter 2. This sequence evaluates the ability of the proposed topology to manage faults affecting both the power sources and the two inverter sides.

Following the first fault, namely the short circuit in Inverter 1, the motor current increases sharply and becomes distorted. The speed decreases from 1500 rpm to 1270 rpm, while the torque and current exhibit large oscillations. The first FT mechanism isolates the faulty leg of Inverter 1 and uses the remaining healthy legs together with the auxiliary switches to form a neutral point. In addition, the DC supply associated with the faulty inverter is connected in series with the second DC supply. This reconfiguration restores the speed to its reference value and brings the currents and torque back close to their pre-fault levels.

When the second fault occurs, corresponding to the failure of DC_1, the faulty supply is isolated and the system continues operating with Inverter 2 and DC_2 in a delta-connected configuration. Under this reduced-power mode, the speed stabilizes at 1470 rpm, the current magnitude decreases, and the torque oscillations remain limited.

The third fault, an open-circuit fault in Inverter 2, causes the speed to drop to 1250 rpm and produces a distorted current surge accompanied by strong torque instability. The third FT mechanism then reconfigures the motor for two-phase operation by isolating the faulty A-phase and using phases B and C. The phase displacement differs from the 180° condition associated with a simple phase loss and is sufficient to generate an RMMF. The controlled neutral point established during the first fault provides a ZSC path and prevents the remaining phases from behaving as a single winding.

After the final reconfiguration, the motor speed stabilizes at 1460 rpm, the currents recover their sinusoidal shape, and the electromagnetic torque remains close to its pre-fault steady-state level, although with slightly reduced performance compared with the pre-fault condition. These results show that the proposed FT strategy can preserve motor operation under a severe sequential fault condition involving both inverters and a DC supply. The corresponding simulation results are presented in Figures 31–33.

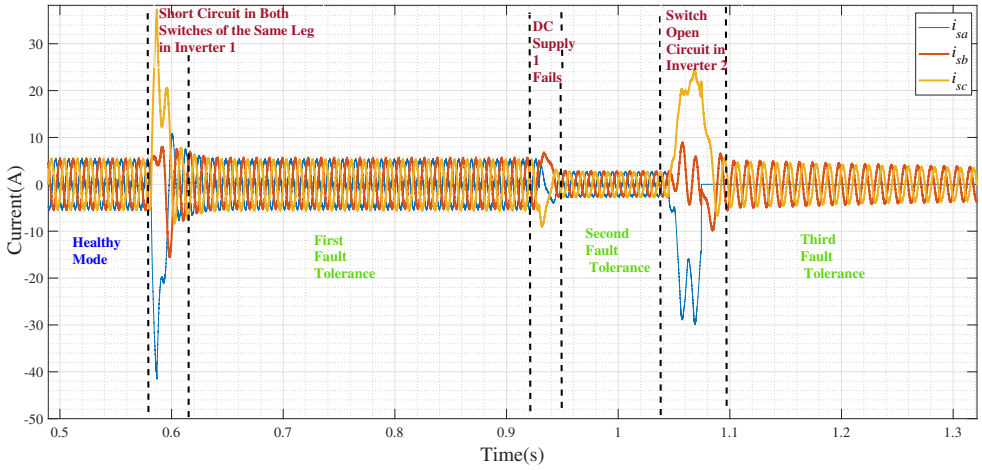


Figure 31. Stator current waveform under combined DC supply fault and faults in both inverters.

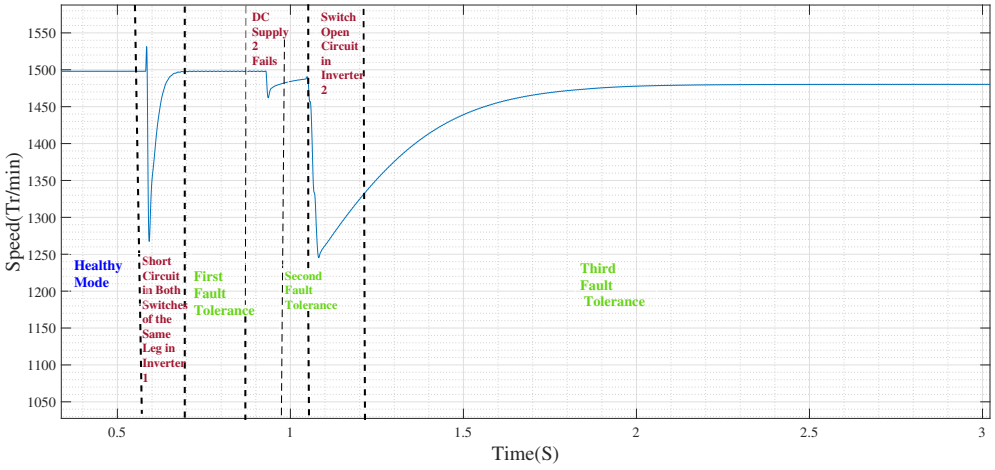


Figure 32. Rotor speed response under combined DC supply fault and faults in both inverters.

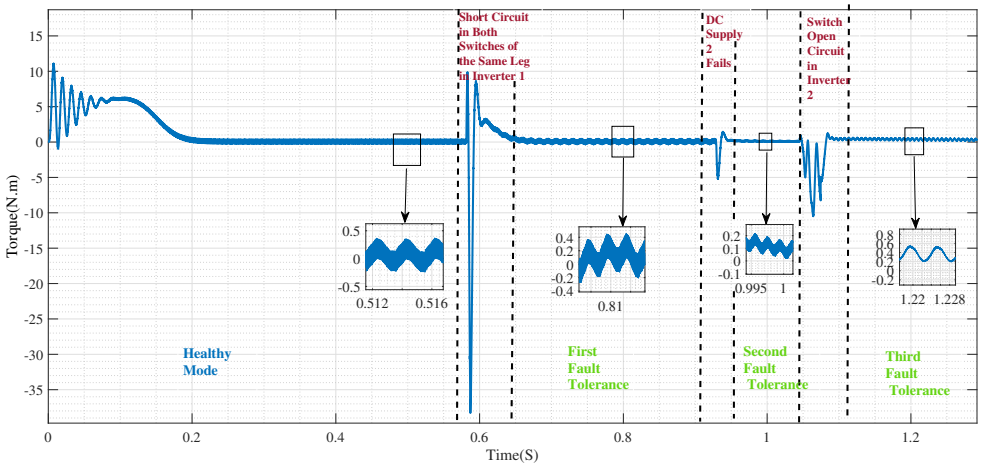


Figure 33. Electromagnetic torque response under combined DC supply fault and faults in both inverters.

4.4. Faults in Both Inverters

This scenario evaluates the FT operation of the proposed topology under two sequential inverter faults. The first fault is an open-circuit fault in switch S_{11} of Inverter 1. It causes the speed to drop below the 1450 rpm reference and produces a 400% surge in distorted currents, accompanied by significant torque oscillations. Activating the first FT mechanism restores stability by isolating DC_1 from the faulty Inverter 1, connecting it in series with the second DC supply, and reconfiguring the faulty inverter as a neutral point. This allows the motor to operate in a star configuration with full rated power capability (100%P_n) and restores the speed, current, and torque close to their pre-fault reference values.

After recovery from the first fault, a second open-circuit fault occurs in switch S_{21} of Inverter 2. This fault causes a 600% current surge, a speed drop to 400 rpm, and severe torque distortion. The second FT mechanism isolates phase A and transfers the system to two-phase operation using phases B and C. The ZSC path established during the first fault supports balanced current flow in the two-phase configuration. This reconfiguration enables the motor to generate an RMMF, recover the speed near the reference value at 1495 rpm, restore sinusoidal currents, and maintain stable electromagnetic torque under degraded two-phase mode. The corresponding simulation results are presented in Figures 34–36.

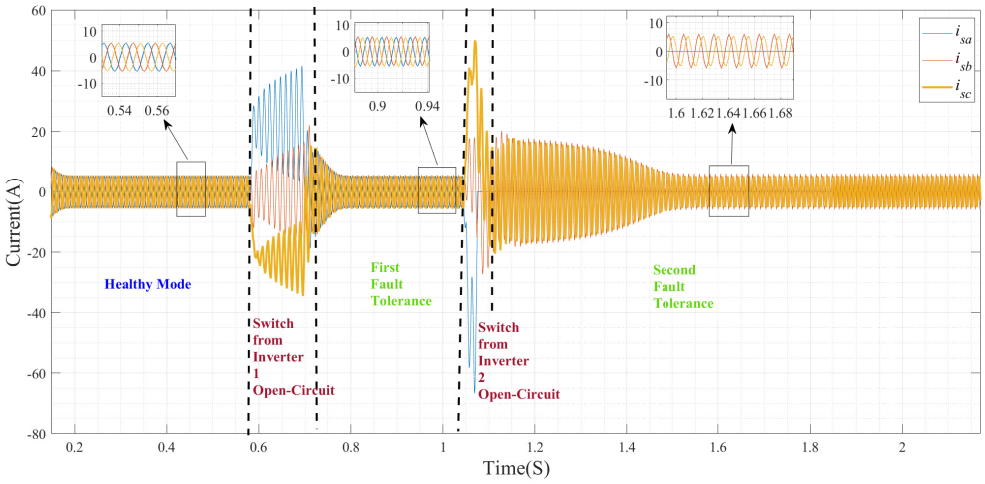


Figure 34. Stator current waveform under faults in both inverters.

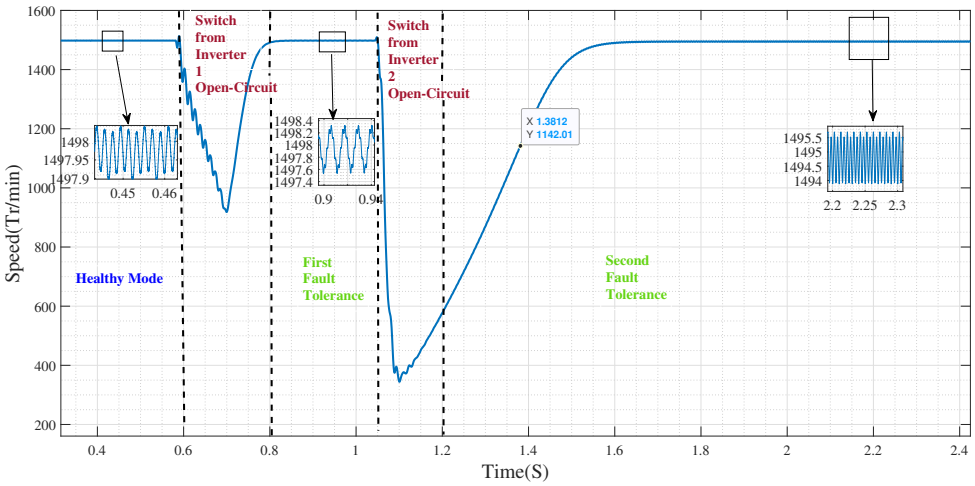


Figure 35. Rotor speed response under faults in both inverters.

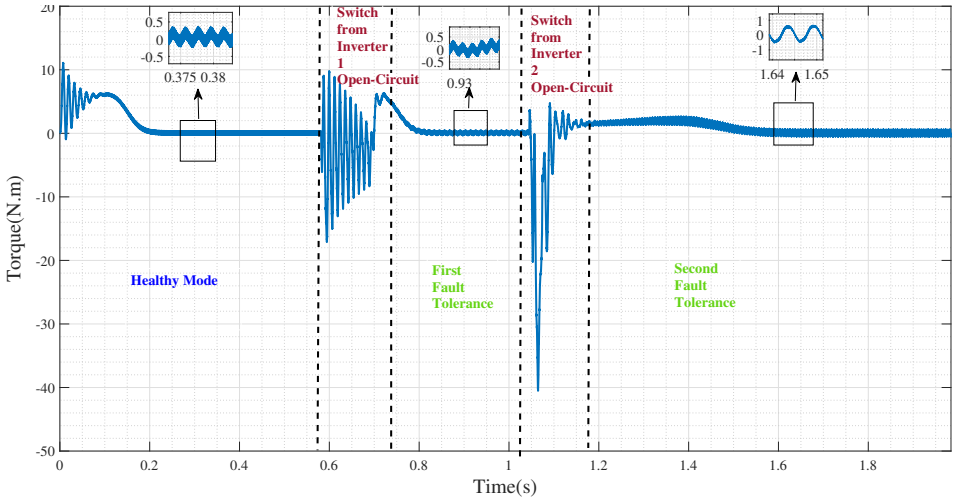


Figure 36. Electromagnetic torque response under faults in both inverters.

4.5. Compound Inverter Fault Under Dynamic Speed and Load Variations

This scenario evaluates the fault-tolerant operation of the proposed OEWIM topology under a compound inverter fault combined with dynamic speed and load variations. The test sequence investigates rated-speed and nominal-torque operation, an inverter fault involving simultaneous open-circuit and short-circuit switch failures, followed by low-speed operation under nominal and reduced loads, dynamic re-acceleration, and an overload condition at 136% of the rated torque.

Initially, the motor operates in the healthy dual-inverter configuration with two separate DC supplies and equal power sharing. The motor accelerates from standstill to the rated speed of 1385 rpm under no-load conditions. At $t = 0.6$ s, the nominal load torque of $T_L = 22.0\ \mathrm{N \cdot m}$ is applied. The speed stabilizes at 1368.1 rpm due to the natural induction motor slip, the electromagnetic torque matches the load demand, and the stator currents are balanced and sinusoidal.

At $t = 0.8$ s, a compound fault is injected into Inverter 2, consisting of an open-circuit fault in the upper switch S_{21} and a simultaneous short-circuit fault in the lower switch S_{25} in different legs. This failure creates an unbalanced operating condition, causing severe torque oscillations and noticeable distortion in the stator currents, while the rotor speed exhibits a sharp drop accompanied by speed oscillations.

At $t = 1.2$ s, the fault-tolerant mechanism is activated. The faulty Inverter 2 is isolated and used to form a neutral point at the motor terminals. Simultaneously, the two separate DC supplies are reconfigured in series to supply the healthy Inverter 1. This reconfiguration transfers the drive to a star-connected single-inverter configuration operating at rated voltage. Following the transition, the torque pulsations are eliminated within 40 ms, three-phase current symmetry is fully restored with balanced sinusoidal waveforms, and the motor speed recovers smoothly to 1368.1 rpm with a dynamic recovery time of $T_{\mathrm{rec}} \approx 50$ ms.

To evaluate dynamic operation under speed variations, the speed reference is ramped down from 1385 rpm to a low speed of 286.5 rpm starting at $t = 1.6$ s while maintaining the nominal load of $T_L = 22.0\ \mathrm{N \cdot m}$. The motor tracks the deceleration trajectory with a smooth torque response and stabilizes at 282.8 rpm with $T_e = 22.2\ \mathrm{N \cdot m}$, confirming stable low-speed operation under nominal mechanical load in the post-fault star configuration.

At $t = 3.0$ s, while operating at low speed, the load torque is reduced from $22.0\ \mathrm{N \cdot m}$ to $10.0\ \mathrm{N \cdot m}$. The electromagnetic torque instantaneously decreases to $10.1\ \mathrm{N \cdot m}$ to balance the new load demand, and the speed stabilizes at 282.9 rpm with balanced three-phase currents.

At $t = 4.0$ s, while maintaining $T_L = 10.0$ N · m, the reference speed is increased from 286.5 rpm back to 1385 rpm. The motor accelerates smoothly and reaches the rated speed at $t = 4.77$ s, stabilizing at 1377.1 rpm. Subsequently, at $t = 5.5$ s, an overload torque of $T_L = 30.0$ N · m (136% of the rated torque) is applied at rated speed. The drive instantaneously develops $T_e = 30.4$ N · m to support the heavy load demand and maintains stable operation at 1362.0 rpm with balanced stator currents, confirming that the reconfigured Star Series-DC mode provides reliable operation across the full torque-speed range. The corresponding simulation results are presented in Figures 37–39.

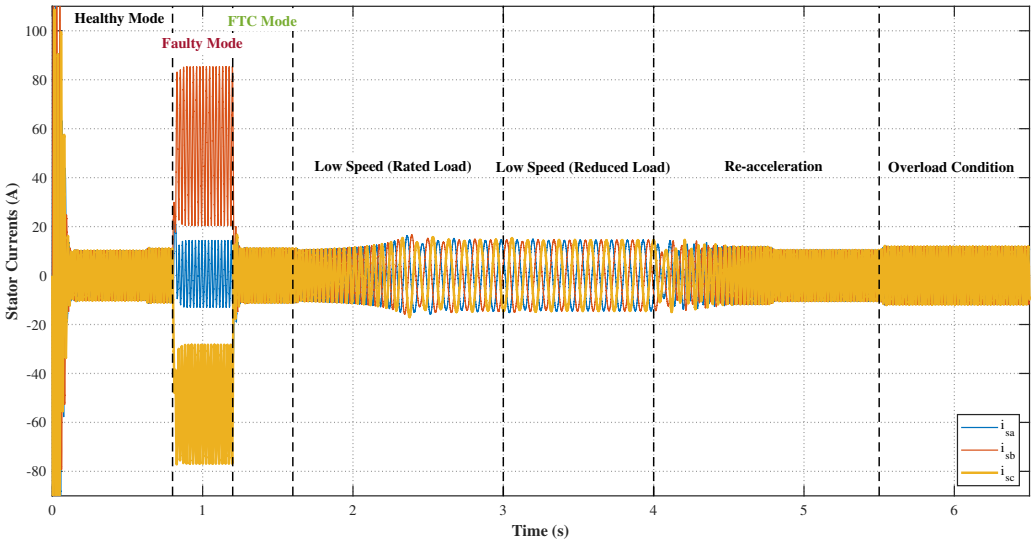


Figure 37. Stator current waveform under a compound inverter fault with dynamic speed and load variations.

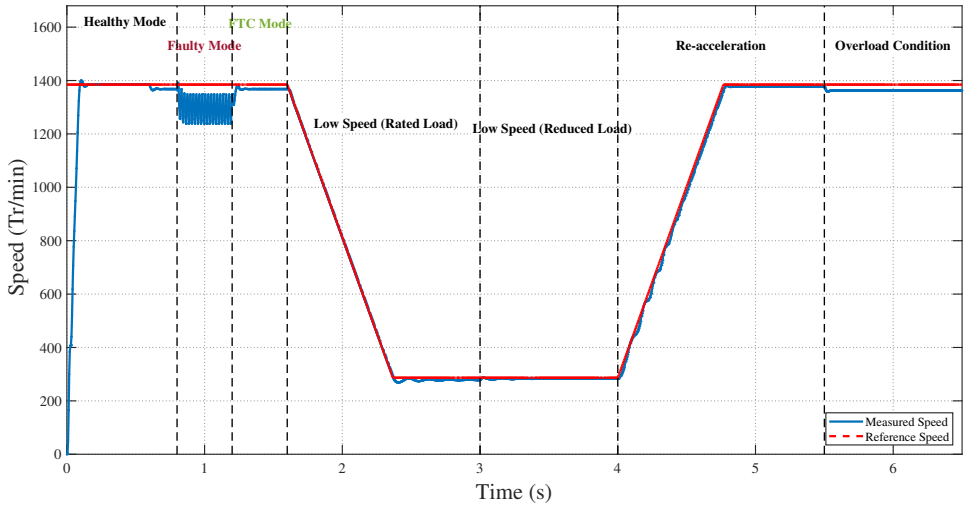


Figure 38. Rotor speed response under a compound inverter fault with dynamic speed and load variations.

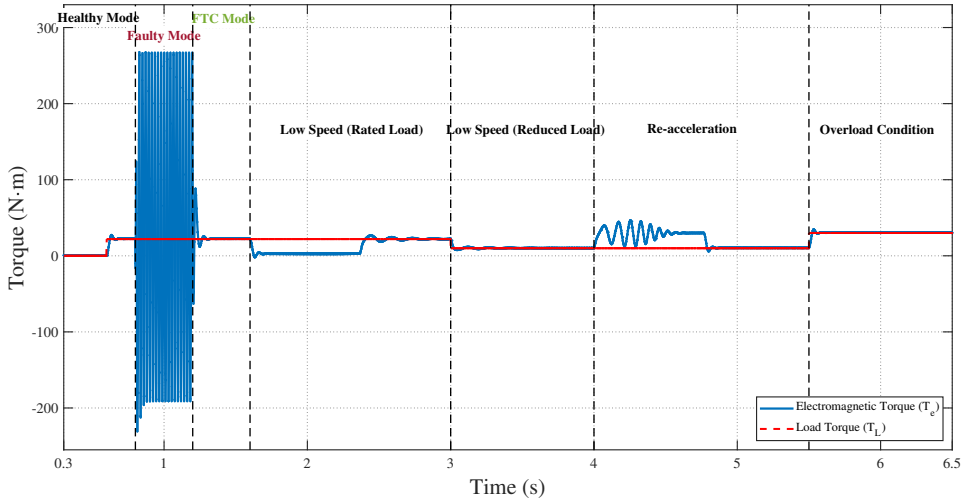


Figure 39. Electromagnetic torque response under a compound inverter fault with dynamic speed and load variations.

4.6. Consecutive Inverter and DC-Supply Faults Under Dynamic Speed and Load Variations

This scenario investigates the resilience and multi-stage fault-tolerant capability of the proposed OEWIM topology under consecutive cross-terminal failures occurring on opposite sides of the machine, combined with dynamic speed and load transitions. The test sequence addresses an inverter switch fault occurring during dynamic acceleration, a post-fault reconfiguration into star mode with series-connected DC supplies, a deceleration to medium speed, a subsequent failure of the opposite DC supply, and a final cross-terminal reconfiguration pairing the healthy inverter with the remaining healthy DC source under nominal mechanical load.

Initially, the drive operates in the healthy dual-inverter configuration with two independent DC supplies in a steady state at a medium speed of 763.9 rpm under no-load conditions. The stator currents are fully balanced and sinusoidal. At $t = 1.20$ s, an acceleration command is initiated to increase the motor speed towards the rated value of 1385 rpm.

During the acceleration transient at $t = 1.30$ s, an open-circuit fault in switch S_{22} occurs in Inverter 2. This failure immediately disrupts the phase voltage synthesis, generating severe torque pulsations spanning over 500 N · m (from -281.9 N · m to $+262.4$ N · m) and causing high current distortion. Consequently, the rotor speed deviates sharply from the acceleration trajectory, dropping temporarily to 728.8 rpm.

At $t = 1.40$ s, the first fault-tolerant control mechanism (FTC 1) is engaged. The faulty Inverter 2 is isolated, its lower switches are configured to establish a neutral point at the machine terminals, and the two DC sources are connected in series to supply the healthy Inverter 1 at full voltage. Following this transition, the electromagnetic torque pulsations are rapidly suppressed within a recovery time of $T_{\text{rec1}} < 45$ ms, balanced sinusoidal currents are restored, and the drive successfully resumes its acceleration, reaching the rated speed of 1384.6 rpm at $t = 1.70$ s.

At $t = 2.00$ s, a partial load torque of $T_L = 5.0$ N · m is applied at rated speed, and the motor stabilizes at 1380.7 rpm with an electromagnetic torque of 5.4 N · m. Subsequently, at $t = 2.60$ s, the speed reference is ramped down back to the medium speed of 763.9 rpm while maintaining the partial load. The motor decelerates smoothly and settles into a steady state at 760.4 rpm with balanced sinusoidal currents.

At $t = 4.00$ s, while operating at medium speed, a major failure occurs in the first DC supply (DC_1), introducing deep voltage distortion and heavy ripple. This second fault

induces substantial torque pulsations (fluctuating between $-72.0\ \mathrm{N \cdot m}$ and $+139.2\ \mathrm{N \cdot m}$), pronounced stator current distortion, and speed perturbations between 732 rpm and 792 rpm.

At $t = 4.40$ s, the second fault-tolerant mechanism (FTC 2) is triggered to address this consecutive cross-terminal failure. The degraded DC_1 source and the previously faulty Inverter 2 are completely isolated. The topology is reconfigured into a cross-terminal single-inverter star configuration, pairing the healthy Inverter 1 with the healthy DC_2 source. The torque and currents recover within $T_{rec2} < 30$ ms, re-establishing balanced sinusoidal operation, while the speed stabilizes at 760.2 rpm. Finally, at $t = 5.00$ s, the nominal load torque of $T_L = 22.0\ \mathrm{N \cdot m}$ is applied. Because the operating speed (763.9 rpm) lies below the base speed of a single DC supply, the single healthy DC source provides nominal flux capability, allowing the motor to develop $T_e = 22.0\ \mathrm{N \cdot m}$ and maintain stable operation at 748.3 rpm with balanced three-phase currents. The corresponding dynamic responses are illustrated in Figures 40–42.

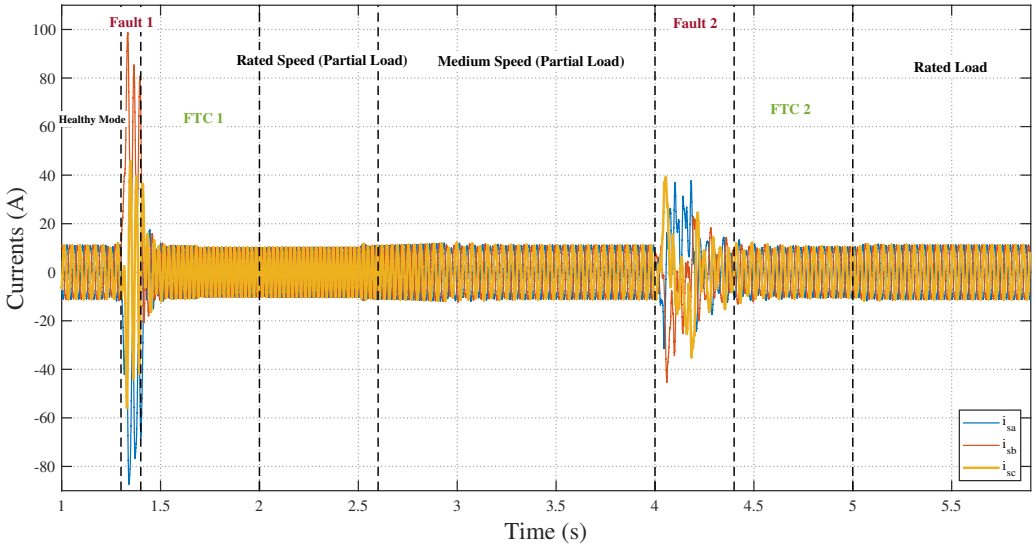


Figure 40. Stator current waveforms under consecutive inverter and DC-supply faults with dynamic speed and load variations.

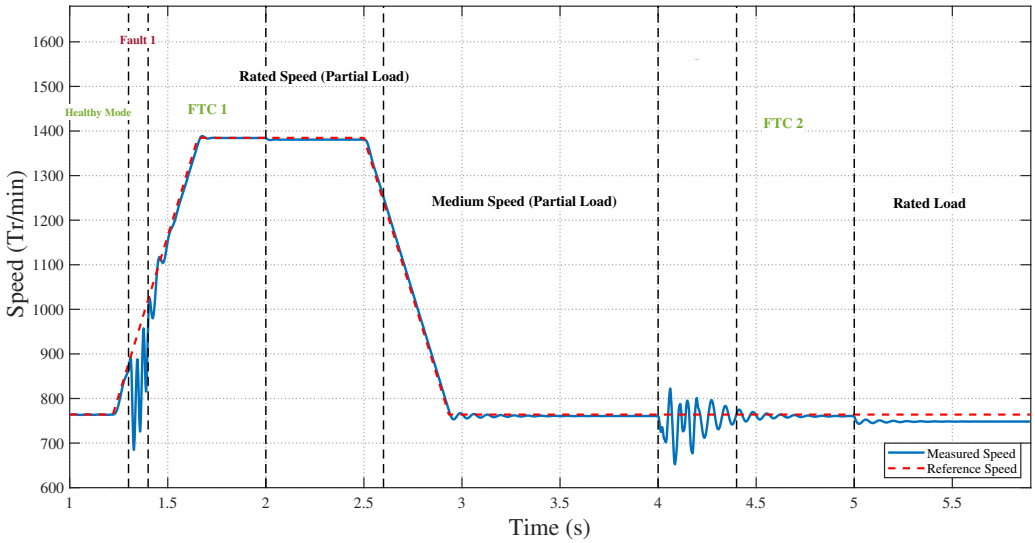


Figure 41. Rotor speed response under consecutive inverter and DC-supply faults with dynamic speed and load variations.

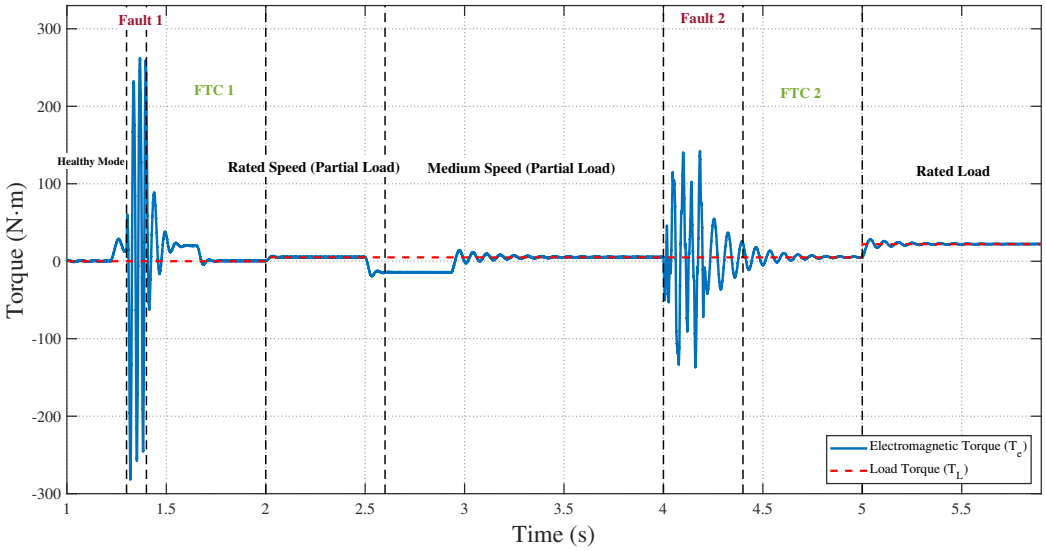


Figure 42. Electromagnetic torque response under consecutive inverter and DC-supply faults with dynamic speed and load variations.

Table 2 compares the proposed strategy with four benchmark fault-tolerant configurations under a baseline single open-switch fault condition. Because machine ratings across the literature vary, the comparative performance metrics are reported using normalized per-unit values and percentage ranges to encompass operation across varying speeds and load conditions.

Table 2. Comparison of different fault-tolerant topologies.

Criterion	Proposed Topology	Benchmark 1 [66]	Benchmark 2 [66]	Benchmark 3 [68]	Benchmark 4 [65]
Post-Fault Stator Mode	Symmetrical 3-phase star	Symmetrical 3-phase star	Asymmetrical 2-phase winding	Symmetrical 3-phase star	Hybrid 3-phase/2-phase with ZSC
DC-Link Utilization	Two DC sources in series	One DC source only (half voltage)	Two DC sources in parallel	One DC source only (half voltage)	Single shared common DC source
Post-Fault Power Capability	Full rated power (100%)	Reduced to half power (50%)	Reduced by thermal limit (57.7%)	Reduced to half power (50%)	Reduced by thermal limit (70.7%)
Stator Current THD	<3.0%	≈3.07%	≈4.05%	≈6.0–7.5%	High (half-wave ZSC bias)
Torque Ripple (ΔT_e)	3.5–5.7%	≈5.0%	10–15%	≈1.2–2.5%	<5% (active ZSC control)
Current Stress (I_{rms}/I_n)	1.0 pu	1.0 pu	1.732 pu	1.0 pu	1.414 pu
Drive Efficiency	High (nominal copper loss)	Moderate	Degraded (high copper loss)	Moderate	Degraded (elevated RMS current)
Fault Recovery Time (T_{rec})	<40 ms (1–2 cycles)	<30 ms	<30 ms	<20 ms	<50 ms (observer settling)
Auxiliary Hardware Overhead	4 auxiliary switches, 2 SPDT contactors	LC impedance networks	LC impedance networks, 2 DC contactors	External output contactors	None (software-based)
Tolerance to Subsequent Faults	Yes (second inverter, DC source, or phase faults)	No (single inverter fault only)	No (single inverter fault only)	No (single inverter fault only)	No (single switch fault only)

The two schemes reported by Li et al. [66] are based on dual boost inverters that incorporate front-end LC impedance networks. In Scheme 1, the faulty inverter is isolated and its healthy lower switches form a neutral point, operating the motor as a three-phase star fed by a single DC source with 50% voltage and power capability. In Scheme 2, only the

faulty phase is isolated while both inverters supply the two healthy phases in a two-phase mode, reaching a thermal limit of 57.7% of rated power.

The method proposed by Lodi et al. [68] also forms a star connection using one inverter and one DC source, resulting in the same 50% power limitation. However, an ANN is used to select the voltage vectors and duty ratios, which reduces the torque ripple to approximately 1.2% at the cost of higher current distortion.

The strategy of Dawara and Muetze [65] takes a different approach by allowing a controlled zero-sequence current to flow through the common DC bus. This avoids any additional hardware, but the resulting half-sinusoidal current waveform increases the RMS current by a factor of $\sqrt{2}$ and introduces significant harmonic distortion.

In contrast, the proposed topology connects the two DC supplies in series and reconfigures the motor into a symmetrical three-phase star. This preserves the full rated voltage and allows the motor to deliver 100% of its rated power with balanced sinusoidal currents. The four auxiliary switches and two SPDT contactors add moderate hardware, but they enable the drive to handle subsequent faults in the DC supplies or the inverters, whether occurring on the same side or across opposite terminals.

Furthermore, these benchmark configurations are physically integrated as individual sub-modes within the proposed dynamic architecture. Consequently, when operating in any corresponding sub-mode, the proposed drive exhibits physical behavior identical to the benchmark at that operating condition. However, existing methods force the drive into early over-isolation by prematurely disabling a healthy DC supply or isolating an entire motor phase. In contrast, the proposed topology preserves full 100% rated power under the baseline fault and reserves degraded sub-modes only as fallback options when multiple faults accumulate. Most importantly, while all the benchmark configurations in Table 2 suffer complete shutdown (0% power) when subjected to subsequent or compound faults, the proposed dynamic architecture maintains stable multi-stage operational continuity.

4.7. Research Challenges and Future Directions

Despite the demonstrated effectiveness of the proposed FT strategy, several challenges remain that require further investigation:

1. Comprehensive and Fast Diagnostic System—This topology requires a real-time diagnostic system capable of detecting and classifying multiple simultaneous faults with high speed and accuracy.
2. Hardware Implementation and Experimental Validation—Although the results confirm the feasibility of the proposed approach, experimental validation on a physical prototype is required to verify its performance under real-world operating conditions.

Addressing these challenges will further enhance the robustness and industrial applicability of FT 3P-OEWIM systems, making them more resilient in safety-critical applications.

5. Conclusions

This paper presented a novel dynamic fault-tolerant topology for 3P-OEWIM drives. By integrating configurations from conventional star motors, common DC supply OEW, and separate DC supplies OEW, the proposed architecture dynamically reconfigures the power routing and switching structure in response to accumulating faults. This adaptive mechanism preserves rated-power operation under single-inverter failures and seamlessly transitions to reduced-power or two-phase operating modes under compound fault conditions.

The unified topology comprehensively manages consecutive and simultaneous faults affecting both inverters and DC sources. Performance evaluations under diverse failure scenarios, including switch open/short circuits and DC link outages, demonstrate stable dynamic recovery and operational continuity.

Overall, the proposed dynamic topology provides a resilient and versatile solution for high-reliability applications such as electric vehicles, industrial automation, and renewable energy systems, ensuring long-term operational continuity under severe fault conditions. The study presented in this paper is currently limited to simulation results. As a continuation and future perspective of this work, the authors plan to conduct experimental validation of the obtained results through three main steps, starting with Processor-in-the-Loop (PIL) testing, followed by Hardware-in-the-Loop (HIL) validation, and ultimately a complete experimental implementation and validation on the physical system.

Author Contributions: Conceptualization, M.L.B., A.B. and A.K.; methodology, M.L.B., A.B. and A.K.; software, M.L.B., A.B. and A.K.; validation, M.L.B., A.B. and A.K.; formal analysis, M.L.B., A.B., A.K. and M.A.; investigation, M.L.B., A.B. and A.K.; resources, M.L.B., A.B. and A.K.; data curation, M.L.B., A.B., A.K. and M.A.; writing—original draft preparation, M.L.B., A.B. and A.K.; writing—review and editing, M.L.B., A.B., A.K., M.A. and J.R.; visualization, M.L.B., A.B., A.K., M.A. and J.R.; supervision, A.K. and M.A.; project administration, A.K., M.A. and J.R.; funding acquisition, M.A. and J.R. All authors have read and agreed to the published version of the manuscript.

Funding: This research received no external funding.

Data Availability Statement: All data used in this study are provided within the paper and its referenced sources.

Acknowledgments: J. Rodriguez acknowledges the support of ANID through project CIA250006.

Conflicts of Interest: The authors declare no conflicts of interest.

Nomenclature

The following abbreviations and symbols are used in this manuscript:

Abbreviations	
(3 + 1)L-NAL	Neutral Connected to an Additional Leg
3L-NCM	Three Legs-Neutral Connected to Capacitor Midpoint
3P	Three-Phase
ANN	Artificial Neural Network
ASC	Active Short-Circuit
CHB	Cascaded H-Bridge
CNN	Convolutional Neural Network
CT	Current Transformation
DC	Direct Current
DTC	Direct Torque Control
EMF	Electromotive Force
EV / EVs	Electric Vehicle(s)
FC	Flying Capacitor
FD	Fault Detection
FDI	Fault Detection and Isolation
FT	Fault Tolerance/Fault-Tolerant
FTC	Fault-Tolerant Control
HIL	Hardware-in-the-Loop
IGBT	Insulated-Gate Bipolar Transistor
IM	Induction Motor
LC	Inductor-Capacitor
MLI/MLIs	Multilevel Inverter(s)
NPC	Neutral Point Clamped
OEW	Open-End Winding
OEWIM	Open-End Winding Induction Motor

Abbreviations	
PIL	Processor-in-the-Loop
PMSM	Permanent Magnet Synchronous Motor
PWM	Pulse-Width Modulation
RMMF	Rotating Magnetomotive Force
RMS	Root-Mean-Square
SNPC	Stator Neutral Point Connection
SPC	Stator Phase Connection
SPDT	Single-Pole Double-Throw
SVPWM	Space Vector Pulse Width Modulation
THD	Total Harmonic Distortion
ZSC	Zero-Sequence Current
Symbols	
P_n	Nominal rated active power (W)
I_n	Nominal rated stator current (A)
I_{rms}	Root-mean-square stator current (A)
T_{rec}	Dynamic fault recovery settling time (s)
ΔT_e	Electromagnetic torque ripple (%)
T_n	Nominal rated electromagnetic torque (N·m)
$v_{abc,s}$	Stator three-phase voltage vector $[v_{as}, v_{bs}, v_{cs}]^T$ (V)
v_{inv1}, v_{inv2}	Output voltage vectors of Inverter 1 and Inverter 2 (V)
v_{a1}, v_{b1}, v_{c1}	Phase leg output voltages of Inverter 1 (V)
v_{a2}, v_{b2}, v_{c2}	Phase leg output voltages of Inverter 2 (V)
$v_{abc,r}$	Rotor three-phase voltage vector $[v_{ar}, v_{br}, v_{cr}]^T$ (V)
$i_{abc,s}$	Stator three-phase current vector $[i_{as}, i_{bs}, i_{cs}]^T$ (A)
$i_{abc,r}$	Rotor three-phase current vector $[i_{ar}, i_{br}, i_{cr}]^T$ (A)
$\hat{i}_{bs}, \hat{i}_{cs}$	Post-fault stator phase currents (A)
$v_{\alpha\beta}, i_{\alpha\beta}$	Stator voltage and current vectors in $\alpha\beta$ stationary frame
V_{dc}, V_{dc1}, V_{dc2}	DC-link supply voltages of shared and separate sources (V)
$\text{DC}, \text{DC}_1, \text{DC}_2$	Direct current power supplies
$\lambda_{abc,s}, \lambda_{abc,r}$	Stator and rotor flux linkage vectors (Wb)
$\lambda_{\alpha\beta}$	Stator flux linkage vector in $\alpha\beta$ stationary frame (Wb)
$\hat{\lambda}_{\alpha s}, \hat{\lambda}_{\beta s}$	Post-fault stator flux components in $\alpha\beta$ stationary frame (Wb)
L_{ss}, L_{rr}	3×3 stator and rotor inductance matrices (H)
L_{sr}, L_{rs}	3×3 mutual inductance matrices between stator and rotor (H)
L_s, L_r	Stator and rotor phase self-inductances (H)
L_{ls}, L_{lr}	Stator and rotor phase leakage inductances (H)
L_m	Magnetizing inductance (H)
M_s, M_r	Stator and rotor inter-phase mutual inductances (H)
R_s, R_r	Stator and rotor phase winding resistances (Ω)
T_e, T_L	Electromagnetic torque and load torque (N·m)
ω_r	Rotor angular speed (rad/s)
J	Rotor moment of inertia (kg·m^2)
F	Viscous friction coefficient (N·m·s)
P	Number of pole pairs
S_n, V_n, f	Rated power (VA), rated voltage (V), and fundamental frequency (Hz)
K	Clarke transformation matrix
I_3, J_3	3×3 identity matrix and 3×3 matrix of ones
S_{ij}	Inverter power semiconductor switches ($i \in \{1,2\}, j \in \{1,\ldots,6\}$)
S_3, S_4, S_5, S_6	Auxiliary bidirectional reconfiguration switches
$\text{SPDT}_1, \text{SPDT}_2$	Single-pole double-throw DC reconfiguration contactors

Appendix A. Induction Motor Parameters

Table A1. Motor Parameters.

Parameter	Value
Rated Power (S_n)	4000 VA
Rated Voltage (V_n)	400 V
Frequency (f)	50 Hz
Number of Pole Pairs (P)	2
Stator Resistance (R_s)	1.405 Ω
Rotor Resistance (R_r)	1.395 Ω
Stator Leakage Inductance (L_{ls})	0.005839 H
Rotor Leakage Inductance (L_{lr})	0.005839 H
Magnetizing Inductance (L_m)	0.1722 H
Moment of Inertia (J)	0.131 kg·m^2
Friction Coefficient (F)	0.002985 N·m·s

References

1. Du, Y.; Zhao, W.; Hu, Y.; Ji, J.; Tao, T. Review of Fault-Tolerant Control for Motor Inverter Failure with Operational Quality Considered. *CES Trans. Electr. Mach. Syst.* **2024**, *8*, 202–215. [CrossRef]
2. Zhang, B.; Dong, Z.; Huang, R.; Liu, C. Reconfigurable Open-End Winding Motor Drive Topology for Inverter Short-Circuit Fault Tolerance. *IEEE Trans. Power Electron.* **2025**, *40*, 3854–3860. [CrossRef]
3. Abdo, A.; Siam, J.; Abdou, A.; Shehadeh, H.; Mustafa, R. Practical Test on the Operation of the Three-Phase Induction Motor under Single-Phasing Fault. *Appl. Sci.* **2024**, *14*, 4690. [CrossRef]
4. Chen, L.; Wang, H.; Tang, Y.; Ma, Y.; Wen, S.; Geda, M.W. IWOA-Optimized Deep Learning for Bearing Fault Diagnosis Under Noisy and Variable Conditions. *IEEE Trans. Instrum. Meas.* **2025**, *74*, 3555218. [CrossRef]
5. Jin, T.; Sun, W.; Zhang, G.; Wang, G.; Jiang, D.; Li, D.; Xu, D. Zero Speed Sensorless Scheme for PMSM Drives Using Virtual Flux Signal Injection Based Hybrid Active Flux Observer. *IEEE Trans. Ind. Electron.* **2026**, *73*, 6657–6668. [CrossRef]
6. Liu, T.-H.; Fu, J.-R.; Lipo, T.A. A strategy for improving reliability of field-oriented controlled induction motor drives. *IEEE Trans. Ind. Appl.* **1993**, *29*, 910–918. [CrossRef]
7. Lü, K.; Dong, X.; Liu, L.; Hu, W.; Nian, H. The Unified Modulation Scheme of Open-End Winding PMSM with Common DC Bus under the Open-Phase Fault Considering the Suppression of Zero-Sequence Current. *Trans. China Electrotech. Soc.* **2020**, *35*, 2387–2395. [CrossRef]
8. Gajanayake, C.J.; Bhangu, B.; Nadarajan, S.; Jayasinghe, G. Fault tolerant control method to improve the torque and speed response in PMSM drive with winding faults. In *Proceedings of the 2011 IEEE Ninth International Conference on Power Electronics and Drive Systems, Singapore, 5–8 December 2011*; IEEE: Piscataway, NJ, USA, 2011; pp. 956–961. [CrossRef]
9. Zhao, Y.; Lipo, T.A. An approach to modeling and field-oriented control of a three phase induction machine with structural imbalance. In *Proceedings of the Applied Power Electronics Conference (APEC '96), San Jose, CA, USA, 3–7 March 1996*; IEEE: Piscataway, NJ, USA, 1996; Volume 1, pp. 380–386. [CrossRef]
10. Correa, M.B.R.; Jacobina, C.B.; da Silva, E.R.C.; Lima, A.M.N. An induction motor drive system with improved fault tolerance. *IEEE Trans. Ind. Appl.* **2001**, *37*, 873–879. [CrossRef]
11. Bolognani, S.; Zordan, M.; Zigliotto, M. Experimental fault-tolerant control of a PMSM drive. *IEEE Trans. Ind. Electron.* **2000**, *47*, 1134–1141. [CrossRef]
12. Ribeiro, R.L.A.; Jacobina, C.B.; Lima, A.M.N.; da Silva, E.R.C. A strategy for improving reliability of motor drive systems using a four-leg three-phase converter. *Proc. IEEE Appl. Power Electron. Conf. Expo. (APEC)* **2001**, *1*, 385–391. [CrossRef]
13. Mendes, A.M.S.; Cardoso, A.J.M. Fault-Tolerant Operating Strategies Applied to Three-Phase Induction-Motor Drives. *IEEE Trans. Ind. Electron.* **2006**, *53*, 1807–1817. [CrossRef]
14. Eickhoff, H.T.; Seebacher, R.; Muetze, A.; Strangas, E.G. Post-Fault Operation Strategy for Single Switch Open Circuit Faults in Electric Drives. In *Proceedings of the 2016 IEEE Energy Conversion Congress and Exposition (ECCE), Milwaukee, WI, USA, 8–22 September 2016*; IEEE: Piscataway, NJ, USA, 2016; pp. 1–6. [CrossRef]
15. Tousizadeh, M.; Che, H.S.; Selvaraj, J.; Rahim, N.A.; Ooi, B.-T. Performance Comparison of Fault-Tolerant Three-Phase Induction Motor Drives Considering Current and Voltage Limits. *IEEE Trans. Ind. Electron.* **2019**, *66*, 2639–2648. [CrossRef]
16. Zhou, X.; Sun, J.; Li, H.; Lu, M.; Zeng, F. PMSM Open-Phase Fault-Tolerant Control Strategy Based on Four-Leg Inverter. *IEEE Trans. Power Electron.* **2020**, *35*, 2799–2808. [CrossRef]

17. Cui, P.; Zheng, Z.; Fu, J.; Zhang, Q.; An, L. A Fault-Tolerant Control Method for a PMSM Servo Drive System with a Four-Leg Inverter. *Electronics* **2023**, *12*, 3857. [CrossRef]
18. Saffar, E.; Ghanbari, M.; Ebrahimi, R.; Jannati, M. A simple fault-tolerant control method for open-phase three-phase induction motor drives. *Control Eng. Pract.* **2023**, *136*, 105525. [CrossRef]
19. Liu, B.; Shi, T.; Yan, Y.; Zhang, G.; Xia, C. Open-Circuit Fault Diagnosis Method for Inverters Based on Critical Characteristics of Half-Wave Current. *IEEE Trans. Power Electron.* **2025**, *40*, 12280–12294. [CrossRef]
20. Pires, V.F.; Salatiel, P.; Cordeiro, A.; Foito, D.; Pires, A.J.; Martins, J.F.A. A New MSCSA Technique for Induction Motor Diagnosis Based on the Park Transform Approach. *Electronics* **2026**, *15*, 3323. [CrossRef]
21. Zhan, J.; Wang, J.; Diao, N.; Sun, X. A Short-Circuit Fault Diagnosis Method for Three-Phase Current-Source Inverters Using Normalized Phase Current Variation Trends. *Machines* **2026**, *14*, 710. [CrossRef]
22. Zhang, Y.; Liu, Y.; Kang, S.; Wang, P. Current Vector Phase Based Weak Open-Circuit Fault Diagnosis of Voltage-Source Inverters. *IEEE Trans. Power Electron.* **2026**, *41*, 9502–9512. [CrossRef]
23. Liu, Z.; He, J.; Jiang, D.; Sun, X.; Yang, G.; Liu, H.; Li, P.; Qu, R. A Hybrid Desaturation Fast Detection Circuit for Bridge Leg Short-Circuit Faults. *IEEE Trans. Power Electron.* **2024**, *39*, 9221–9229. [CrossRef]
24. Zhao, J.; Cheng, S.; Wu, X.; Li, W.; Wang, D. A Dual-Branch Network-Based Method for Unified Diagnosis of IGBT Open-Circuit and Current Sensor Faults in Three-Phase Inverters. *IEEE Trans. Power Electron.* **2026**, *41*, 17747–17762. [CrossRef]
25. Lei, X.; Wu, F.; Liu, Y. An Online Convolutional Neural Network Based Method for Open-Circuit Fault Diagnosis in Three-Phase Inverters Under Extremely Unbalanced Loading Condition. *IEEE Trans. Power Electron.* **2026**, *41*, 16084–16098. [CrossRef]
26. Fang, M.; Yan, W.; Wang, W. Real-Time On-MCU Open-Circuit Fault Diagnosis of Electric-Vehicle Inverters Using a Lightweight Angular Sector-Energy Network. *World Electr. Veh. J.* **2026**, *17*, 357. [CrossRef]
27. Gatla, R.K.; Kumar, D.G.; Shashavali, P.; Rao, D.S.N.M.; Kotb, H.; Alkuhayli, A.; Ghadi, Y.Y.; Mbasso, W.F. Comprehensive analysis of faults and diagnosis techniques in cascaded multi-level inverters. *Heliyon* **2024**, *10*, e39901. [CrossRef] [PubMed]
28. Huang, Z.; Yang, T.; Giangrande, P.; Galea, M.; Wheeler, P. Technical review of dual inverter topologies for more electric aircraft applications. *IEEE Trans. Transp. Electrif.* **2022**, *8*, 1966–1980. [CrossRef]
29. Zerdani, M.; Chafouk, H.; Ardjoun, S.A.E.M. Performance Analysis of a Dual-Inverter-Fed Open-End Winding Induction Machine under Asymmetrical Control: Theoretical Approach and Experimental Validation. *Symmetry* **2024**, *16*, 395. [CrossRef]
30. Zerdani, M.; Ardjoun, S.A.E.M.; Chafouk, H. Overview of Dual Two-Level Inverter Configurations for Open-End Winding Machines: Enhancing Power Quality and Efficiency. *Appl. Sci.* **2025**, *15*, 5611. [CrossRef]
31. Nayli, A.; Guizani, S.; Ben Ammar, F. Experimental Analysis for Star and Open-End Stator Winding Structures of IM. *Power Electron. Drives* **2025**, *10*, 271–286. [CrossRef]
32. Lakhimsetty, S.; Satelli, V.S.P.; Rathore, R.S.; Somasekhar, V.T. Multilevel torque hysteresis-band based direct-torque control strategy for a three-level open-end winding induction motor drive for electric vehicle applications. *IEEE J. Emerg. Sel. Topics Power Electron.* **2019**, *7*, 1969–1981. [CrossRef]
33. Mizukoshi, A.; Haga, H. Improvement of output voltage waveform in dual inverter fed open-winding induction motor at low speed area. In *Proceedings of the 2018 IEEE Energy Conversion Congress and Exposition (ECCE), Portland, OR, USA, 23–27 September 2018*; IEEE: Piscataway, NJ, USA, 2018; pp. 5422–5427. [CrossRef]
34. Kodumur Meesala, R.E.; Kunisetti, V.P.K.; Thippiripati, V.K. Enhanced Predictive Torque Control for Open End Winding Induction Motor Drive Without Weighting Factor Assignment. *IEEE Trans. Power Electron.* **2019**, *34*, 503–513. [CrossRef]
35. Lodi, K.A.; Beig, A.R.; Al Jaafari, K.A.; Aung, Z. ANN-Based Improved Direct Torque Control of Open-End Winding Induction Motor. *IEEE Trans. Ind. Electron.* **2024**, *71*, 12030–12040. [CrossRef]
36. Kimura, T.; Yamada, T.; Kazaoka, R.; Noguchi, T. Control Method of a Dual Inverter System for EV with One Battery. In *Proceedings of the 2022 International Power Electronics Conference (IPEC-Himeji 2022—ECCE Asia), Himeji, Japan, 15–19 May 2022*; IEEE: Piscataway, NJ, USA, 2022; pp. 31–38. [CrossRef]
37. Qasim, M.M.; Otten, D.M.; Lang, J.H.; Kirtley, J.L.; Perreault, D.J. Comparison of Inverter Topologies for High-Speed Motor Drive Applications. *IEEE Trans. Power Electron.* **2024**, *39*, 7404–7422. [CrossRef]
38. Sudarshan Reddy, K.; Baskar, S. A Literature Review on Open End Windings Induction Motor Drives. In *Proceedings of the 2021 5th International Conference on Electrical, Electronics, Communication, Computer Technologies and Optimization Techniques (ICEECCOT), Mysuru, India, 10–11 December 2021*; IEEE: Piscataway, NJ, USA, 2021; pp. 395–398. [CrossRef]
39. Adame Najera, E.Z.; De León Aldaco, S.E.; Aguayo Alquicira, J.; Lozoya-Ponce, R.E.; Pecina-Sánchez, J.Á.; Portillo Contreras, S. A Survey on Topologies and Modulation Strategies of Dual Inverters in Industrial Applications. *Eng* **2025**, *6*, 316. [CrossRef]
40. Zeng, Z.; Goetz, S.M. A General Modeling and Analysis of Impacts of Unbalanced Inductance on PWM Schemes for Two-Parallel Interleaved Power Converters. *IEEE Trans. Power Electron.* **2024**, *39*, 12235–12248. [CrossRef]
41. Li, Q.; Zhang, Z.; Huang, Y.; Li, J.; Zhang, X.; Yuan, C. Component-Reuse Hybrid Filter Design for Effective Leakage Current Suppression in Parallel Inverter Motor Drive Systems. *IEEE Trans. Power Electron.* **2026**, *41*, 17139–17153. [CrossRef]

42. Shen, Z.; Liu, Y.; Yang, S.; Sun, X.; Lin, F.; Cheng, M. A Novel Zero-Sequence Current Elimination PWM Scheme for an Open-Winding PMSM with Common DC Bus. *IEEE Trans. Power Electron.* **2019**, *34*, 12476–12490. [CrossRef]
43. Shen, Z.; Jiang, D.; Chen, J.; Qu, R. A Novel Zero-Sequence Current Elimination PWM Scheme for an Open-End Winding Motor Drive with Dual Two-Level Inverter. In *Proceedings of the 2018 IEEE Applied Power Electronics Conference and Exposition (APEC), San Antonio, TX, USA, 4–8 March 2018*; IEEE: Piscataway, NJ, USA, 2018; pp. 1679–1686. [CrossRef]
44. Zhang, S.; Zhou, Y.; Li, X.; Zhang, C. An Improved Modulation Strategy with Torque Ripple Suppression Method for OEW-PMSM Drives with Common DC Bus. *IEEE Trans. Transp. Electrif.* **2023**, *9*, 3095–3105. [CrossRef]
45. Zhan, H.; Zhu, Z.Q.; Odavic, M. Analysis and Suppression of Zero Sequence Circulating Current in Open Winding PMSM Drives with Common DC Bus. *IEEE Trans. Ind. Appl.* **2017**, *53*, 3609–3620. [CrossRef]
46. Yao, L.; Yang, S.; Xie, Z.; Zhang, X. Eliminating Scheme of Zero-Sequence Currents in Open-End Winding Induction Motor Drive with a Single DC Power Supply. In *Proceedings of the 2017 Chinese Automation Congress (CAC), Jinan, China, 20–22 October 2017*; IEEE: Piscataway, NJ, USA, 2017; pp. 3538–3543. [CrossRef]
47. Lee, K.; Han, Y. Simple Discontinuous Pulse-Width Modulation Scheme for the Loss Reduction of a Dual Inverter Fed an Open-End Winding Induction Motor. *IEEE Trans. Energy Convers.* **2023**, *38*, 495–506. [CrossRef]
48. Hu, W.; Ruan, C.; Nian, H.; Sun, D. Zero-Sequence Current Suppression Strategy with Common-Mode Voltage Control for Open-End Winding PMSM Drives with Common DC Bus. *IEEE Trans. Ind. Electron.* **2021**, *68*, 4691–4702. [CrossRef]
49. Zhu, B.; Rajashekara, K.; Kubo, H. Predictive Torque Control with Zero-Sequence Current Suppression for Open-End Winding Induction Machine. In *Proceedings of the 2015 IEEE Industry Applications Society Annual Meeting, Addison, TX, USA, 18–22 October 2015*; IEEE: Piscataway, NJ, USA, 2015; pp. 1–7. [CrossRef]
50. Zou, Z.; Yang, S.; Zhang, Y.; Zhang, X. Research on Fault-Tolerant Control Strategy of Open-End Winding Drive with a Common DC Bus Under a Switch Open-Circuit Fault. *CPSS Trans. Power Electron. Appl.* **2024**, *9*, 230–241. [CrossRef]
51. Kedika, N.R.; Pradabane, S. Fault-Tolerant Multi-Level Inverter Topologies for Open-End Winding Induction Motor Drive. *Int. Trans. Electr. Energ. Syst.* **2021**, *31*, e12718. [CrossRef]
52. Jia, Y.-F.; Zhang, L.; Li, Z.; Liu, W.; Zhang, Y.; Zhang, W.; Li, S.; Liang, X.; Song, J. Control Strategy for an Open-End Winding Induction Motor Drive System for Dual-Power Electric Vehicles. *IEEE Access* **2020**, *8*, 8844–8860. [CrossRef]
53. Srinath, V.; Mohan, M.; Chaturvedi, D.K. A Multilevel Inverter System for an Induction Motor with Open-Ended Windings. *Int. J. Comput. Appl.* **2017**, *163*, 6–13. [CrossRef]
54. Lakhimsetty, S.; Surulivel, N.; Somasekhar, V.T. Improvised SVPWM Strategies for an Enhanced Performance for a Four-Level Open-End Winding Induction Motor Drive. *IEEE Trans. Ind. Electron.* **2017**, *64*, 2750–2759. [CrossRef]
55. Reddy, B.V.; Somasekhar, V.T. A SVM based four-level open-end winding-induction motor drive with voltage balancing of DC-link capacitors using SVM based HCC front-end converter. In *Proceedings of the Annual IEEE India Conference, Hyderabad, India, 16–18 December 2011*; IEEE: Piscataway, NJ, USA, 2011; pp. 1–5. [CrossRef]
56. Kim, T.-H.; Lee, J.-H.; Yoon, B.-R.; Lee, J.-S. Clamping Modulation Technique for Balancing Power Losses of Dual Inverter with Isolated DC Bus. *IEEE Access* **2023**, *11*, 41868–41879. [CrossRef]
57. Zhang, G.; Liu, Y.; Gu, X.; Liu, B.; Chen, W. Technical Review of Dual-Inverter Fed Open-End Winding Motor System. *IEEE Trans. Transp. Electrif.* **2026** , Early Access. [CrossRef]
58. Jeon, J.-H.; Lee, K.-B. A Fault Diagnosis for OEW-IPMSM Drives Fed by Common DC Bus using High-Frequency Injection. In *Proceedings of the 2026 International Power Electronics Conference (IPEC-Nagasaki 2026—ECCE Asia), Nagasaki, Japan, 31 May–4 June 2026*; IEEE: Piscataway, NJ, USA, 2026; pp. 1–5. [CrossRef]
59. Yang, S.; Sun, X.; Ma, M.; Zhang, X.; Chang, L. Fault Detection and Identification Scheme for Dual-Inverter Fed OEWIM Drive. *IEEE Trans. Ind. Electron.* **2020**, *67*, 6112–6123. [CrossRef]
60. Matsumori, H.; Maeda, Y.; Kosaka, T.; Matsui, N. Open Device Fault Detection and Fail Safe Action Strategy for a Premium Class Electric Vehicle with a Dual Inverter fed Open Winding Motor. In *Proceedings of the 2021 IEEE Energy Conversion Congress and Exposition (ECCE), Vancouver, BC, Canada, 10–14 October 2021*; IEEE: Piscataway, NJ, USA, 2021; pp. 1527–1533. [CrossRef]
61. Ruan, C.; Hu, W.; Nian, H.; Sun, D. Open-Phase Fault Control in Open-Winding PMSM System with Common DC Bus. In *Proceedings of the 2019 IEEE Applied Power Electronics Conference and Exposition (APEC)m Anaheim, CA, USA, 17–21 March 2019*; IEEE: Piscataway, NJ, USA, 2019; pp. 1052–1056. [CrossRef]
62. Chakrabarti, A.; Saha, A.; Biswas, S.K. Winding Open-Circuit Fault-Tolerant Operation of Single DC-Link Dual-Inverter Fed Three-Phase Open-End Induction Motor Drive. *IET Power Electron.* **2021**, *14*, 1256–1270. [CrossRef]
63. Lv, K.; Dong, X.; Zhu, C. Research on Fault-Tolerant Operation Strategy of Permanent Magnet Synchronous Motor with Common DC Bus Open Winding Phase-Breaking Fault. *Energies* **2022**, *15*, 2927. [CrossRef]
64. Huang, S.; Luo, G.; Liu, C.; Zhao, Y.; Chen, Z. Fault-Tolerant Method of Current Reconstruction for Open-end Winding Permanent Magnet Synchronous Machine Electric Propulsion System with Open-Phase Operation. *IEEE Trans. Transp. Electrif.* **2026**, Early Access. [CrossRef]

65. Dawara, A.A.; Muetze, A. Post-Fault Control Strategy of Open-Winding Machines Under Inverter Open-Circuit Fault with Torque Ripple Reduction. In *Proceedings of the 2026 International Power Electronics Conference (IPEC-Nagasaki 2026—ECCE Asia), Nagasaki, Japan, 31 May–4 June 2026*; IEEE: Piscataway, NJ, USA, 2026; pp. 1–6. [CrossRef]
66. Li, C.; Wang, G.; Li, H.; Li, F.; Xia, Z.; Liu, Z. Fault-Tolerant Analysis of Two Boost Inverters for Open-End Winding Induction Motor Drives. *J. Power Electron.* **2021**, *21*, 647–659. [CrossRef]
67. Muduli, U.R.; Beig, A.R.; Jaafari, K.A.; Alsawalhi, J.Y.; Behera, R.K. Interrupt-Free Operation of Dual-Motor Four-Wheel Drive Electric Vehicle Under Inverter Failure. *IEEE Trans. Transp. Electrif.* **2021**, *7*, 329–338. [CrossRef]
68. Lodi, K.A.; Beig, A.R.; Jaafari, K.A.A. ANN-Based Fault-Tolerant Control of Open-End Winding Induction Motors for Electric Vehicles. In *Proceedings of the 2025 IEEE/AIAA Transportation Electrification Conference and Electric Aircraft Technologies Symposium (ITEC+EATS), Anaheim, CA, USA, 18–20 June 2025*; IEEE: Piscataway, NJ, USA, 2025; pp. 1–6. [CrossRef]
69. Lodi, K.A.; Al Jaafari, K.A.; Poshtan, M.; Dekka, A.; Beig, A.R. Improved Fault-Tolerant Control of Open-End Winding Induction Motor for Electric Vehicle Applications. In *Proceedings of the 2025 IEEE Energy Conversion Congress and Exposition (ECCE), Philadelphia, PA, USA, 19–23 October 2025*; IEEE: Piscataway, NJ, USA, 2025; pp. 1–6. [CrossRef]
70. Sun, X.; Liu, Z.; Jiang, D.; Qu, R.; Liu, H.; Yang, G. An Active Control Method After Switch Short-Circuit Fault for Open-End Winding Motor System with Isolated Supply. In *Proceedings of the 25th European Conference on Power Electronics and Applications (EPE'23 ECCE Europe), Aalborg, Denmark, 4–8 September 2023*; IEEE: Piscataway, NJ, USA, 2023; pp. 1–7. [CrossRef]
71. Sun, X.; Wang, J.; Qian, M. Space-Vector Analysis of Open-end Winding Motor Drive with Isolated Supply Under Switch Short-Circuit Fault. In *Proceedings of the 2025 5th International Conference on Electrical Engineering and Control Science (IC2ECS), Beijing, China, 5–7 December 2025*; IEEE: Piscataway, NJ, USA, 2025; pp. 693–696. [CrossRef]
72. Meinguet, F.; Kestelynx, X.; Semailx, E.; Gyselinck, J. Fault detection, isolation and control reconfiguration of three-phase PMSM drives. In *Proceedings of the 2011 IEEE International Symposium on Industrial Electronics, Gdansk, Poland, 27–30 June 2011*; IEEE: Piscataway, NJ, USA, 2011; pp. 2091–2096. [CrossRef]
73. Béthoux, O.; Labouré, E.; Remy, G.; Berthelot, E. Real-Time Optimal Control of a 3-Phase PMSM in 2-Phase Degraded Mode. *IEEE Trans. Veh. Technol.* **2017**, *66*, 2044–2052. [CrossRef]
74. Wang, Y.; Lipo, T.A.; Pan, D. Robust operation of double-output AC machine drive. In *Proceedings of the 8th International Conference on Power Electronics—ECCE Asia, Jeju, Republic of Korea, 30 May–3 June 2011*; IEEE: Piscataway, NJ, USA, 2011; pp. 140–144. [CrossRef]
75. An, Q.; Wang, G.; Sun, L. A Fault-Tolerant Operation Method of PMSM Fed by Cascaded Two-Level Inverters. In *Proceedings of the 7th International Power Electronics and Motion Control Conference (IPEMC 2012—ECCE Asia), Harbin, China, 2–5 June 2012*; IEEE: Piscataway, NJ, USA, 2012; pp. 1310–1313. [CrossRef]

Disclaimer/Publisher's Note: The statements, opinions and data contained in all publications are solely those of the individual author(s) and contributor(s) and not of MDPI and/or the editor(s). MDPI and/or the editor(s) disclaim responsibility for any injury to people or property resulting from any ideas, methods, instructions or products referred to in the content.